SIMULATION STUDY OF FIN-STRUCTURE MICRO-LASER BASED ON III-NITRIDE MATERIAL

A Thesis

by

CHEN GONG

Submitted to the Office of Graduate and Professional Studies of
Texas A&M University
in partial fulfillment of the requirements for the degree of

MASTER OF SCIENCE

Chair of Committee,	Harlan Rusty Harris
Committee Members,	Alexey Belyanin
	Pao-Tai Lin
	Samuel Palermo
Head of Department,	Miroslav M. Begovic

May 2018

Major Subject: Electrical Engineering

Copyright 2018 Chen Gong

ABSTRACT

Interconnect bottleneck in integrated circuit industry is brought about by complexity of structure, upper boundary of bandwidth, parasitic capacitors of parallel links, and distortion and interference as the distance between copper lines goes smaller and smaller. This problem, potentially, can be solved by photonic integrated circuit (PIC) technology, yet optical components are far less matured to reach chip level. We put forward a planar structure PIC which is based on fin-structure technology and focused on the design and simulation study of the laser source: III-Nitride fin-structure micro-laser (FSML).

Compared with conventional semiconductor lasers such as vertical cavity surface emitting diodes (VCSELs) and edge emitting diodes lasers (EELDs) etc., footprints of FSMLs are much smaller, and the threshold current density is promising to be dramatically reduced. Even though III-Nitride optoelectronic devices are suffering from the limitation of substrate options and defect-density, these drawbacks can largely be overcome due to the fin-structure design. In terms of photonic integrated circuits (PICs) applications, the compatibility of FSML is better than traditional light sources (LEDs, VCSELS, EELDs) because of the less coupling loss with waveguide. We started our work with electrical study of fin-LED design, and followed with optical/multi-physics study on DBRs, cavities, and laser-modelling. In chapter1, we give a brief review of the development of light sources applied in IC industries and compare the performance of different material systems. Chapter

2 focuses on the design of separate components of FSML (DBRs, LEDs, cavities, waveguides). The laser modelling is a highly complex work, which is detailly described in chapter 3; laser performance and data analysis are also included in this chapter. The last chapter presents a summary of the simulation work, and possible future direction in PhD program. Software skills required in this thesis include COMSOL multi-physics, MATLAB, Autodesk Inventor, and Microsoft Office software.

ACKNOWLEDGEMENTS

Fortunately, at this moment, I'm at the beginning of my academic career thanks to the spiritual and financial support of my parents, the academic environment of University of Electronic Science and technology of China (UESTC) and Texas A&M University, love and miss of my girlfriend, the help of all members in our team, the guidance of Dr. Harris, and the patience of all committee members. I'm deeply grateful for the arrangement of fate, and the given opportunity to make efforts. The most attractive part of the fate is not that all our wishes come true; instead, it is the unpredictable combination of circumstances. Like most dream-chasers, I desired to find a golden stepping-stone that would send me to the gate of heaven directly, yet unluckily, I'm always treading on thin ice, and gradually, I started to realize, life is consist of imperfection, and the sense of discontentment pushes me to a new level, and till that time, I will be able to see all the steps I have survived through are golden. I entered UESTC in 2012; it is not the top few comprehensive universities in China, yet at least, it is a member of "985 project" universities and ranked at the top in the field of electrics and communication. Teachers in our departments were wonderful; they are patient, and warm-heart, and considerate. Dr. Zhong, Jian and Dr. Wang, Jun had great influence on my academic interest. Thanks to Dr. Zhong's acceptance, I joined his group, and started to learn organic electric materials and designed and fabricate my first OPV device. The project I did in his group greatly broaden my knowledge: there is a kind of electric thin film that can be

printed on regular building glasses and generate electricity power when sun shines, it looks like a technology that can save the world which is now dominantly driven by fossil fuel. It's a good thing for me if I focus on the research of OPV, yet I'm curious about other applications of optoelectronics. I entered Dr. Wang's group at the end year of my undergraduate period, and there I learned terahertz detection based on graphene. In his group, I did more fabrication issues such as graphene exfoliation, lithography, lift-off, metal deposition. Another harvest for me in UESTC was an exchange program to UCSB, funded by China Scholarship Council, so at the beginning of the 2016, I stayed in Santa Barbara and waited my graduate program admissions. I took Professor Steven P. DenBaars' solid state class in UCSB, yet I didn't know who that man was, but later, when I started my FSMLs project in TAMU, I read a lot of literatures of him. If I knew what I would do in the future, I must work harder in his class. In that exchange program, I shared an apartment with a girl, who also came from UESTC as an exchange student. Somehow, I felt a sense of happiness when I prepared meals and had a walk on the beach with her in the evening. I said goodbye with her with great dismay at the moment of parting at the end exchange program: She gave up graduate programs in America and decided to go Hong Kong University of science and technology, yet I accepted the admission from TAMU. It took us half a year after the program to realize that the happiness was unshaped love, and we decided to be "together" no matter how wide the Pacific Ocean is.

My life in Texas was started from the summer of 2016, and my first advisor is Dr. Lin Pao-tai. In his group, I learned a lot of fabrication skills and optical considerations, which contribute directly to my later research. I planned to do further research related to optics in his group, yet eventually, I decided to insist on my optoelectronic focus. Luckily, Dr. Harris gave me that opportunity, and I entered for his group to study on LEDs and VCSELs and always believe optoelectronics will lead to a revolution just like how IC changed the world in last century. Dr. Harris is very patient on research, he recommended me to carry out my research one step after another and compare apple to apple; as an experienced researcher, he taught me how to pursue perfect in every detail.

That is my memory since undergraduate time; I will have a very difficult way to go, yet I'm confident because of the help and support of so many people. In the next several years, I will continue my study on this field and focus on its applications on display and communication and sensing, and further, I would like to do R & D or processing jobs in an Integrated Circuit Design and Manufacture (IDM) company. My girlfriend is applying graduate study in the USA now, and hopefully, she will come to TAMU in the fall of 2018.

In all, I'm on the way to my academic career with the help of a lot of people, especially my advisor, Dr. Harris, and other professors serving for my thesis committees. Thanks to the help of all members in our group that I can get some progress, and thanks to all peoples who love me that I'm confident to overcome difficulties in study and life. Fortunately, I'll

get my Master of Science Degree, yet that is just a start: The revolution has not been accomplished; comrades still have a long way to struggle through!

Chen Gong,

01/20/2018, College Station

CONTRIBUTORS AND FUNDING SOURCES

Contributors

This work was supervised by a thesis committee consisting of Dr. Harlan Rusty Harris, Dr. Pao-tai Lin and Dr. Samuel Palermo of the department of Electrical & Computer Engineering, and Dr. Alexey Belyanin of the department of Physics & Astronomy. All work for this thesis was completed independently by the student under the advisement of Harris, Harlan Rusty of the department of Electrical and Computer Engineering.

Funding Sources

There are no outside funding contributions to acknowledge related to the research and compilation of this document.

TABLE OF CONTENTS

ABSTRACT....................ii

ACKNOWLEDGEMENTS....................iv

CONTRIBUTORS AND FUNDING SOURCES....................viii

TABLE OF CONTENTS....................ix

LIST OF FIGURES....................xi

LIST OF TABLES....................xiii

1. INTRODUCTION....................1

1.1. Development and Applications....................3
1.1.1. Semiconductor Light Sources....................3
1.1.2. VCSEL-Based Transceivers for Data Communications....................6
1.1.3. VCSEL-Based Parallel Links....................9
1.2.Fin-Structure Micro-Laser application....................13
1.2.1. Fin-Structure Devices....................13
1.2.2. FSMLs-Based Parallel Links Technology....................16
1.3.Material Systems....................18
1.3.1. Long wavelength VCSELs....................18
1.3.2. III-Nitride VCSELs....................20
References....................21

2. FSML DESIGN....................26

2.1. LED Designs....................28
2.1.1. 1-D simulation....................28
2.1.2. 2-D simulation....................31
2.2. Distributed Bragg Reflectors (DBRs) Designs....................32
2.2.1. The Transmission Matrix Method....................33
2.2.2. Reflection Spectra....................34
2.3. Cavity Designs....................36
2.3.1. Standing Wave Condition....................36
2.3.2. Absorption of III-Nitride Materials in Cavity....................38
2.4. Waveguide Simulation....................40
2.4.1. 1-D Model for Planer Waveguide Simulation....................41

2.4.2. 3-D Model for Rib Waveguide Simulation.....42
References.....47

3. FSML MODELLING AND DATA ANALYSIS.....48

3.1. Optical Gain.....48
3.1.1. Gain and Absorption in Laser Media.....48
3.1.2. Gain in MQW Lasers.....50
3.2. A General Method for Semiconductor Laser Modelling.....53
3.2.1. Effective Extinction Coefficient.....54
3.2.2. "Pure Optical" Model.....57
3.3. Performance of One/Two/Three-MQW FSML.....58
3.3.1. Quality Factor of FSMLs Spectrum.....58
3.3.2. Threshold Current of FSMLs.....61
References.....63

4. CONCLUSION AND FUTURE DIRECTION.....64

4.1. Limitations of Simulation Work and Outlook.....64
4.2. Further Plan: Research Focus in PhD Period.....65

LIST OF FIGURES

Page

Figure 1 Energy gap of the III-V materials…………………..…………………………..… 6

Figure 2 The cross-section of VCSEL-based silica fiber transceiver package…….……..… 8

Figure 3 Data rate and cost…………………………………………………………….… 8

Figure 4 Cross-section of PETIT module, ultimate version……………………….…… 11

Figure 5 Cross-section of Terabus link………………………………………………12

Figure 6 Hybrid Silicon Photonic Integrated Circuit………………………………..… 12

Figure 7 Cross-section of n-MOSFET……………………………………………….… 14

Figure 8 Cross-section of n-CMOS……………………………………………………. 14

Figure 9 Typical Fin-FET…………………………………………………………….… 15

Figure 10 Parallel links based on Fin-Structure Micro-Laser……………………….… 17

Figure 11 3-D structure of FSML……………………………………..………..… 26

Figure 12 Cross-section of fin-structure LED……………………….……..……..… 27

Figure 13 Band structure and carrier distribution of one/two/three-QW LEDs………..… 30

Figure 14 General performances of LEDs………………………………………….… 31

Figure 15 Reflectance spectra of DBRs...……………………………………………..…35

Figure 16 Reflective index of materials………………………………………………. 35

Figure 17 Q-factor and Resonance frequency……………………………………….… 40

Figure 18 Waveguide mode........ 42

Figure 19 Energy distribution in waveguides........ 44

Figure 20 Spontaneous emission in direct semiconductor........ 49

Figure 21 Principles of semiconductor laser........ 49

Figure 22 Modal gain (1/m) of QWs in currents........ 51

Figure 23 Modal gain of bulk GaN laser (left) and QW GaN laser(right)........ 53

Figure 24 Flow chart physical description of laser model........ 55

Figure 25 Average effective extinction coefficient of QWs........ 56

Figure 26 Spectrum output of laser........ 59

Figure 27 FWHM vs. Current Density........ 60

Figure 28 Quality factor vs. Current Density........ 61

Figure 29 Laser power output as a function of current density........ 62

Figure 30 Light propagating in device........ 65

LIST OF TABLES

Page

Table 1 The development of ICs from 2001 to 2012.. 1

Table 2 Necessary parameters for LED design.. 29

Table 3 Quantified LED design for 1-D simulation... 29

Table 4 Laser design.. 39

1. INTRODUCTION

With the development of lithography technology, the validness of Moore's law has been maintained, and the semiconductor industry seems to be confident till today. The reduction on the feature size of CMOS device has brought about higher device switching speed and faster circuits. However, this positive trend fades if we take into account interconnection network in integrated circuits (ICs). Difficulties come from complexity of structure, upper boundary of bandwidth, parasitic capacitors between parallel links, and distortion and interference as the distance of copper lines goes smaller and smaller. Table 1 measures the development of ICs from the view of chip size, complexity, and data rate, and as it presents, the gap between on-chip local clock and data rate on peripheral buses increases as time goes by, and that is interconnect bottleneck.

Table 1. The development of ICs from 2001 to 2012, reprinted from [27]

YEAR OF FIRST PRODUCT SHIPMENT	*2001*	*2003*	*2006*	*2009*	*2012*
TECHNOLOGY GENERATIONS (nm)	*150*	*130*	*100*	*70*	*50*
CHIP SIZE (mm^2)					
Microprocessor	385	430	520	620	750
ASIC	850	900	1000	1100	1300
CHIP COMPLEXITY					
Transistors/chip (Microprocessor)	40 M	76 M	200 M	520 M	1.40 B
Max Interconnect Length (meters/chip)	2,160	2,840	5,140	10,000	24,000
Chip I/Os	2,400	3,000	4,000	5,400	7,300
PERFORMANCE (MHz)					
On-chip local clock	1,500	2,100	3,500	6,000	10,000
On-chip, across-chip clock	1,400	1,600	2,000	2,500	3,000
Chip-to-board speed, high performance	1,400	1,600	2,000	2,500	3,000
Chip-to-board peripheral buses	785	885	1,035	1,285	1,540

A potential solution for this crisis is the application of photonic integrated circuits (PICs), where some electric components are selectively replaced by optical components. PIC is significant for the development of modern communication for two reasons: first, it is potential to relief the increasing of power consumption of traditional COMS integrate circuit resulted from smaller feature sizes and larger leakage current; and second, it supports faster processor, and satisfies the increasing demand for bandwidth across servers, boards and on-chip due to the large transmission rate and high modulation bandwidth [1]. Main optical components in PIC includes (but are not limited on) light sources, modulators, optical amplifiers, photodetectors, filters and waveguides, switches and MEMS. Even though the blueprint is so beautiful, optical components and links are far less matured to reach chip level even in today. Fibers, although widely used in cables, are too large for chips; lens and mirrors increase the complexity of circuits; mixing optical and electrical components on one chip leads to unacceptable cost. All these issues add obstacles for the spread of PICs.

Conventionally, the fabrication of PIC is based on silicon-on-insulator (SOI) technology, which is costly compared with planar fabrication. In this research, we take advantage of fin-structure to put forwards a planar structure for PICs, which will be described in detail in section 1.2. Correspondingly, optical devices on such a PIC are all in fin-structures such as fin-laser, fin-detector fin-waveguide and fin-SOA (semiconductor optical amplifier). Not only does this technology reduce the 3D circuit problem to be a 2D problem, it shrinks the footprint of optical components as well. Potentially, it is able to

achieve low-cost PICs, easy-fabrication process and on/off-chip multi-GHz- bandwidth communication.

Although it is exciting to illustrate the whole construction of the new PIC and devices on it, the work to achieve it should be started from the terminal: fin-laser source. Only after this step, we will be able to work on signal propagation and reception, and modulation. Therefore, the design and simulation of an efficient laser source is the priority first for me to do. In order to be compatible with the new PIC based on fins, fin-structure micro-laser (FSML) is presented, and it shares a lot of features in common with surface cavity semiconductor emitting laser (VCSELs).

1.1. Development and Applications

1.1.1. Semiconductor Light Sources

Traditionally, three types of light source are promising in photonic integrated circuit: edge-emitting laser diodes (EELDs), vertical cavity semiconductor lasers (VCSELs), and light emitting diodes (LEDs) although, none of them are perfect. Relatively speaking, VCSELs are most potential among these three candidates: compared with EELDs, VCSELs have lower threshold current, higher efficiency, slower divergent, lower cost, and simpler mounting and packaging process; while compared with LEDs, VCSELs have higher modulation bandwidth, more focused output beam, narrower spectrum, smaller operating current and higher power efficiency [2]. Because of these favorable features, VCSELs are worthwhile for enthusiastic investigation.

The development of VCSELs was started from 1977, by Prof. Kenichi Iga, and the first publication shows up in Dec. 1979, based on the material of GaInAsP/InP [3]; in the year of 1984, Iga et al., obtained a room-temperature pulsed operation in VCSEL based on AlGaAs/GaAs [4]. However, the threshold current was high because of the insufficient reflective index of reflectors and small gain regions of VCSELs. In order to enhance the reflectivity and reduce the threshold current, great efforts were focused on mirror materials and structures. A ring electrode which was separated from the mirror in 1984 [5] and Au/SiO_2 and dielectric multilayer mirrors in 1986 [6] was applied by Uchiyama et al. Multiple dielectric layers of SiO_2/TiO_2 were firstly applied in VCSELs on n-side (output side) in 1987 by Kinoshita et al., and the threshold current was reduced to 6mA [7]. In early research, an obvious observation is that GaInAsP/InP based VCSELs only works at low temperature, and AlGaAs/GaAs VCSELs can be operated in room temperature, which shows wider applications. The room temperature continuous wave operation of VCSELs were presented in 1988 by Koyama et al., and after the early efforts on VCSELs, groups in AT&T, UCSB, and Bellcore joined this field.

On the other hand, the combination of DBRs and VCSELs was started from 1985 by Chailertvanitkul [8] and Sakaguchi in 1988 [9], and this thin multilayer structure can be obtained by more advanced deposition technology such as MOCVD, which dramatically improves the surface morphology and promotes the further development of VCSELs. In the research of T.E.Sale, VCSELs design and fabrication are described detailly, and one

unavoidable problems of DBR-VCSELs is the high resistance of Bragg Reflector [10]. In his research, n and p type DBRs are the injection layers of electrons and holes with high potential barriers for carriers. Another part of valuable work, in his research, is the combination of quantum wells (QWs) with VCSELs and the gain calculation of QWs, which is instructive for laser modelling.

So far, the spectrum of all VCSELs in literatures above ranges from red to infare, based on GaInAsP/InP and AlGaAs/GaAs. III-Nitride VCSELs were born much later, and till now, they are far less developed compared with the previous two due to the limitations on proper substrates, P-type doping efficiency, and density of defects. However, the demand of light source based on GaN and its alloy, such as $In_xGa_{1-x}N$ and $Al_xGa_{1-x}N$, is increasing especially in display technology: semiconductor light sources with the spectrum from blue to violet were rare until the birth of GaN-based homojunction LED by Akasaki et al., in 1994 [11] and high-bright InGaN/GaN double-heterostructure LED by Nakamura et al., in 1994 [12]. Figure 1 presents energy gap of the III-V as a function of lattice parameter; GaInAsP/InP and AlGaAs/GaAs systems can only achieve the spectrum from green to infare, while spectrum of III-Nitride materials covers the whole visible range. Later, III-Nitride alloys were applied in multi-quantum-well edge-emitting lasers, and the device lifetime was expanded to 10000 hours with the power output of 420mW by 1998 [13]. After that, III-Nitride edge emitting laser found its industry position such as high density optical storage system and went to commercialization rapidly.

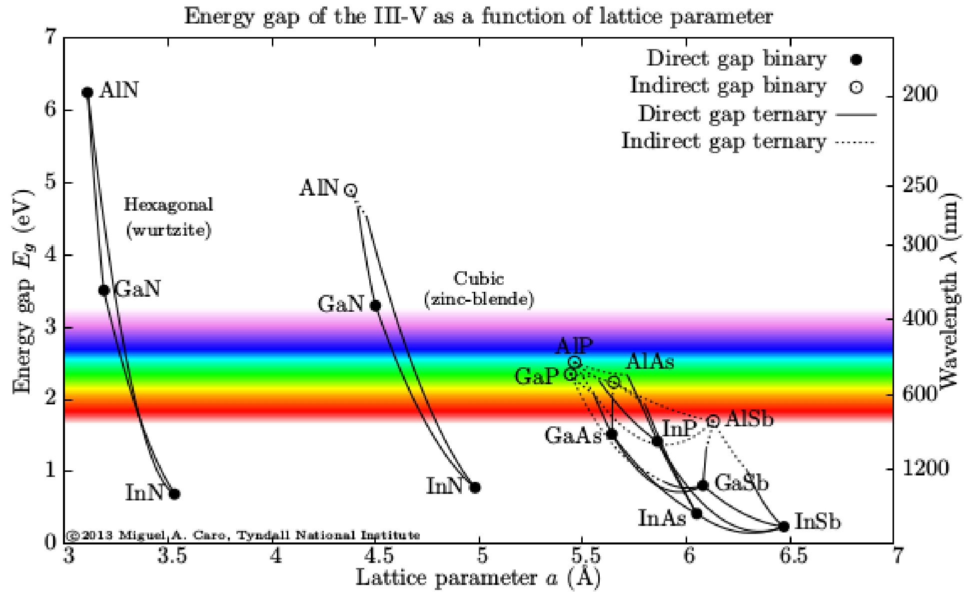

Figure 1. Energy gap of the III-V materials, reprinted from [28]

Despite of its success on edge emitting laser, III-Nitride materials developed slowly in VCSEL applications, and till now, the commercialization of III-Nitride VCSEL is far from accomplished. However, the demands for such product is growing in illumination, display, optical communication, and photonic integrated circuits, etc. Till the year of 2013, VCSELs (based on all materials) enjoyed the second largest production volume among all types of semiconductor lasers and only exceeded by Fabry–Pérot-type edge-emitting lasers.

1.1.2. VCSEL-Based Transceivers for Data Communications

The combination of VCSELs and multimode optical fiber provide a good solution for low-cost optical interconnection, which is attractive for data communication applications such as storage and local area networks (SANs and LANs) as well as system interconnection for high performance computing (HPC).

Fiber-optical interconnection shows its advantages in terms of distance and bulk, and

in early days (mid 1980s), LED is the most developed candidate in this application. However, the limitations on LED transceivers are obvious for two reasons: data rate is bottlenecked around a few hundred Mbit/s, and the large loss in coupling and propagation undermined its applications in long distance communication. Lasers look like a possible solution for these difficulties because of its higher power and greater modulation rates although optimal lasers at that time were expensive for long-distance link. The first generation of laser light source was edge-emitting laser diode (EELD) with optical self-pulsation, which minimized the modal noise in fiber links, and in the next several years, it turned to be the mainstream in short distance data communication industry and pushed the operation speed forward to 531Mbit/s [14].

The competitiveness of EELDs faded in the middle of 1990s when the data speed approached to 1Gbit/s due to the physical limitation on oscillation frequency, in the next generation of data communication transceiver, EELD's position was taken by VCSEL for the higher operation speed and tolerance for larger temperature ranges. VCSELs were inexpensive due to the wafer scale fabrication and testing that they shared a large part of the market fast till today. Figure 2 is the cross-section of VCSEL-based silica fiber transceiver package.

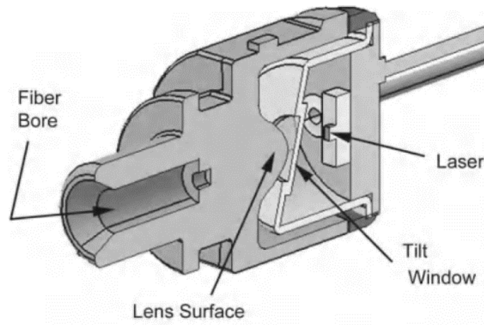

Figure 2. The cross-section of VCSEL-based silica fiber transceiver package, reprinted from [2].

The operating rate of transceiver today is much more enhanced: regularly, it can be 10Gbit/s or even larger with the cost much lower than before. We can predict that 25Gbit/s data rate will be reached within recent couple of years. III-Nitride based VCSEL is more stable in temperature variation than its GaInAsP/InP and AlGaAs/GaAs counterparts, and the shorter wavelength light shows less power loss in the new generation of low cost plastic optical fibers, thus, potentially, it will be the next type of data communication transceiver. Figure 3 (a) present the data rate development, and (b) cost of data transmission.

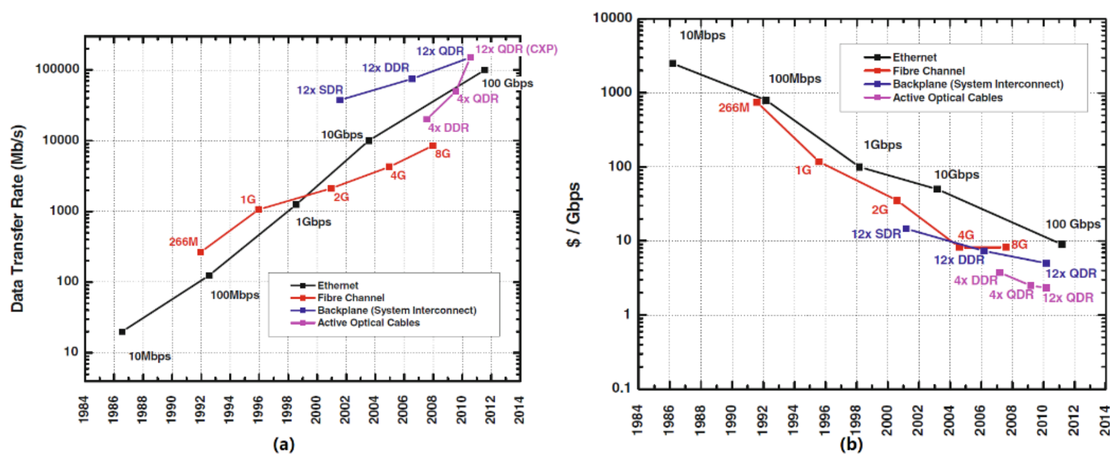

Figure 3. Data rate and cost. (a) data rate development (b) cost for data transmission reprinted from [25]

1.1.3. VCSEL-Based Parallel Links

One of the most attractive applications of VCSEL in IC industry is parallel links, which is promising to selectively replace some electrical components suffering from interconnect bottleneck. Optical parallel links can be understood as optical transceivers in chip level, which is basically consisted of VCSELs (signal sources), waveguides (channels), and photodetectors (receivers). However, this technology has not been fully developed and commercialized since the problems on reliability, manufacturability, cost and volume.

The first commercialized VCSEL-based parallel links were created by HP company in PONI project around the end of 1990s. In early stage, the electrical interfaces of VCSEL-based parallel links were soldered to IC, and transmitter module was separated from receptor module. This product contained 12 channels, and for each channel, the data rate could be as high as 1.25Gbit/s with the wavelength of 850nm. Almost at the same time, IBM was trying to commercialize a 12-channel transceiver based on 850nm VCSELs which was called LITBUS. VCSELs and photodetectors were mounted on a flex bent up to 90° to aligned fibers just like PONI, the difference was that these fibers were mounted in Si V-groove couplers. However, this research was not commercialized because of the fade of fiber optical industry even though the throughput of 15Gbit/s with 12 channels in total was achieved.

The attempts of these two companies were followed by the collaborated research of McGill University and BAE System, in which 256 channels and 1080 850 nm VCSEL-Photodetector pairs were fabricated in an integrated circuit. This research was not successful

since the data rate was low in multichannel operation.

Following POIN project, Agilent laboratories carried out POSH (parallel Optical Super Highway) project, and different from POIN, the 850nm wavelength was replaced by 990 nm wavelength, and optical couplers and heat sinks were changed to lens and heat pipes, respectively. In predication, the data rate should be as high as 10Gbit/s/ch, yet the actual speed was only 9Git/s/ch because of the crosstalk. This was the first time when crosstalk in parallel links draw scientists' attention.

NEC joined to VCSEL parallels competition latter than those previous organizations and started the research on 850nm VCSEL-based transceiver called MCM type OIP. At the beginning, they applied polymer waveguide with 45° mirror as couplers for fibers, which achieved 1.25Gbit/s/ch with six VCSEL-photodetector pairs in total. The effort was exceeded by NEC's PETIT module quickly, which has four VCSEL-photodetector pairs with the speed of 3.25Gbit/s/ch in early version and attained 10Gbit/s/ch eventually. In ultimate version, PIN photodetectors replaced MSM ones and transmitters and receivers and ICs were merged into a single package, which was flip-chip mounted on a resin film, and a micro-lens array was inserted between the resin film and PT connectors. Figure 4 shows the cross section of the ultimate version.

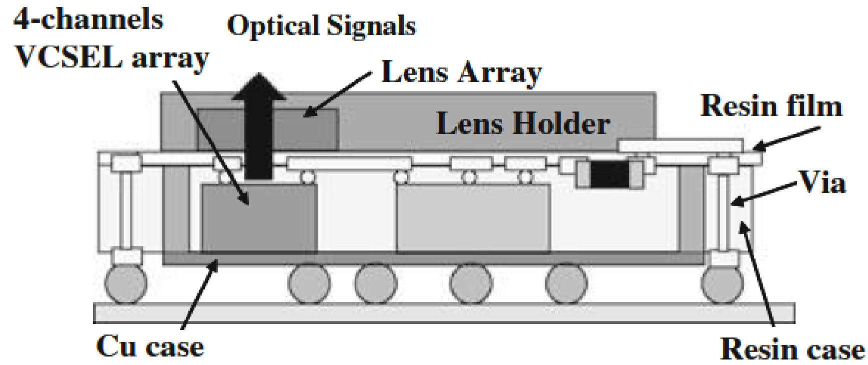

Figure 4. Cross-section of PETIT module, ultimate version, reprinted from [25]

Another attempt researchers carried out was multi-color parallel links, which was demonstrated by Lucent's CWDM project. In their publication [16], four VCSELs with the wavelength of 815nm, 822nm, 829nm, 836nm on one package were achieved, and the data rate was 10Gbit/s/ch. Lawrence Livermore National Laboratory (LLNL) pushed forward this research [17] and a 40-channel parallel link using 825nm, 845nm, 977nm, 988nm wavelength was demonstrated.

IBM, cooperated with Picolight Inc. continued their study of LITBUS to explore the limitations of that early product. This time, they redesigned the flex circuit, and replaced it with SiGe circuits, and later, low-power CMOS which supports the data rate of 10 Gbit/s/ch. More exciting progress was that they achieved over 300m error-free link at the total rate of 120 Gbit/s based on OM3 fiber and error detector. And later, the product of this research, SNAP12 link, with the rate of 10 Gbit/s/ch has been commercialized by Avago Technologies.

Almost at the same time, IBM started another collaboration with Agilent, Terabus project, and in this project, 2D OE array flip-chip soldered on CMOS IC, were mounted on parallel circuit board containing 1D waveguides, lens array, mirror. This process is more

manufacturable and reliable. The first-generation product used Si carrier and separated transmitter and receptor module and was followed by the second generation with organic carrier and transceiver module. The new generation includes two variations: one is high power version with the power consumption of 9mW/Gbit/s at the data rate of 15Gbit/s/ch; another one is the low-power version, 5mW/Gbit/s at the data rate of 10Gbit/s/ch. Ultimately, the commercialized product operated at the wavelength of 850nm with the data rate of 12.5Gbit/s/ch, and 24 channels in total. Figure 5 shows how were Terabus links mounted.

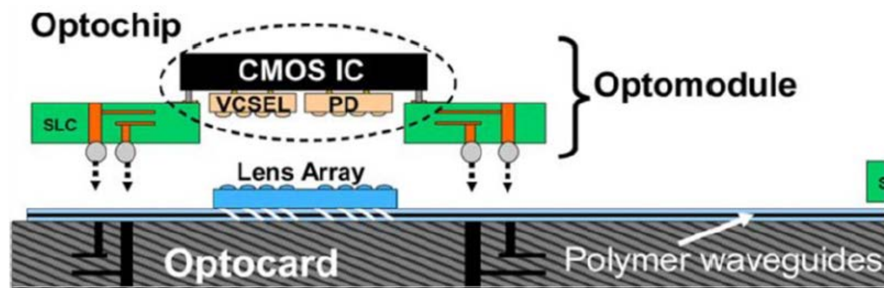

Figure 5. Cross-section of Terabus link, reprinted from [25]

More recently, VCSEL-photodetector pairs have been integrated into integrated circuit on silicon-on-insulator platform, and this technology merges all component on a chip, which is more suitable for IC applications.

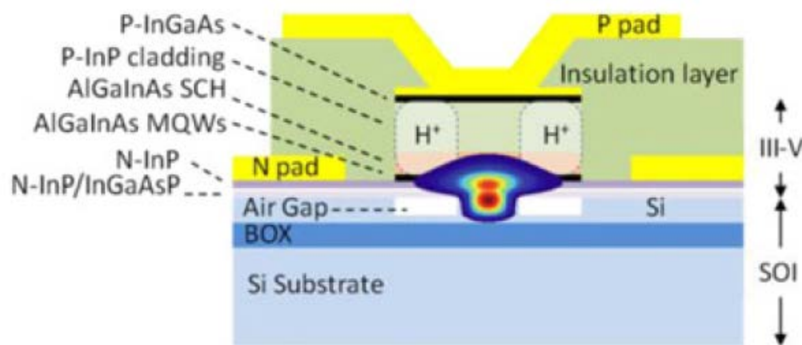

Figure 6. Hybrid Silicon Photonic Integrated Circuit, reprinted from [18]

One typical structure is shown in figure 6, in which light is generated in the VCSEL

above SOI platform and coupled into the waveguide below. Si is almost transparent for infare light so that signals can propagate along the channel to photodetectors, where light signal will be transformed to electrical signals and identified by the following CMOS circuit. Predictably, this technology can be adopted in industry if its complexity and cost can be reduced.

The review of parallel application is ended here, and our effort is the modification on PICs based on parallel links, and the corresponding laser source of the new PIC construction. Instead of devices suspended on SOI platform (shown in figure 9), our parallel links are based on planar structures, which reduces the fabrication complexity and cost.

1.2. Fin-Structure Micro-Laser applications

1.2.1. Fin-Structure devices

Currently, the most matured Fin-Structure device is Fin-FET, which has been commercialized by some IDM (integrated circuit design and manufacture) companies such as Intel already. Being the Savior of Moore’s Law, it changed the traditional 2D device to 3D device, and excellently controls the short channel effect. In this section, I’m going to compare the performance of MOSFET, CMOS, and Fin-FET.

In example of n-MOSFET (shown in figure 7), the drain is grounded, and the source is connected to positive bias. When the positive voltage of gate is small ($V_{GS} < V_{th}$), electron channel below the gate cannot be formed so that there is no current flow, theoretically; yet when the positive bias on gate increases, source and drain can be “connected”, and in this

way, the device can achieve on/off states.

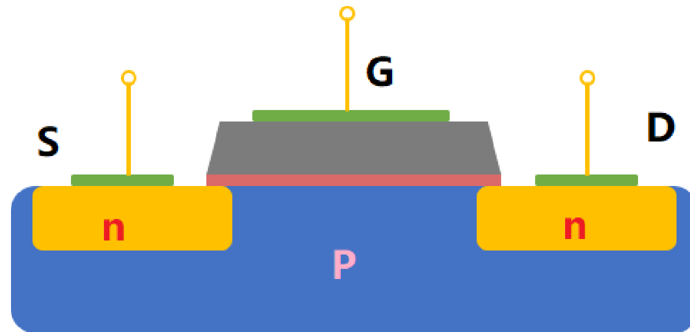

Figure 7. Cross-section of n-MOSFET

However, if the scale of the device shrinks, the current flow at off state cannot be negligible. That is the reason why MOSFET loses its position in integrated circuit gradually today.

The leakage current at off state, which is mentioned above, can be relieved by COMS technology, in which base bias is added to suppress that effect. The leakage of current existed because the source and drain are “weakly connected” when the gate length is extremely small, and the additional base bias compensate the resistance between them. The cross section of CMOS is shown in figure 8. In actual connection, base and source are usually merged and connect to positive voltage bias.

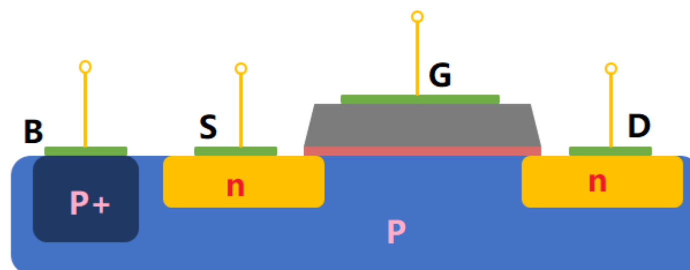

Figure 8. Cross-section of n-CMOS

Nevertheless, during the switching time of the gate voltage goes from one state to another state, device conduct briefly. This give rise to an abrupt spike in power consumption and arise a serious issue at high frequencies [15].

The problems mentioned above, including leak current and power consumption, can be solved by Fin-FET. Unlike conventional MOSFET or CMOS, Fin-FET is an unpolarized 3D device with a wrapped gate across the fin. Figure 9 is a typical Fin-FET.

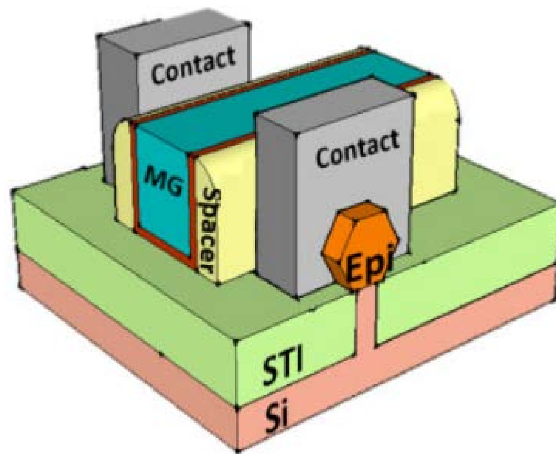

Figure 9. Typical Fin-FET, reprinted from [26]

In this device, the “Epi” region, which is wrapped by two contacts and spacer, “MG”, is the fin; it is grown by epitaxy. The two contacts are source and drain respectively, and the metal gate is “MG” in the plot. In nanometer scale, Fin-FET shows a lot of merits which cannot be shared by its 2D counterparts including suppressed short channel effect, smaller footprint and low-energy consumption. Actually, from 2D to 3D is a big step for integrate circuit, because in 3D world, more fantastic structures can be made, and the device design is going to be more flexible.

1.2.2. FSMLs-Based Parallel Links Technology

The maturity of Fin-FET illuminates the application of fin-structure in integrated circuit, and of course, such a structure can also be transferred to optical components in PICs. In Fin-FET, not only does the fin play the role as a supporting structure, it is the carrier channel as well. In PICs, the fin takes another role as the waveguide, which is the channel for light signals. Unlike SOI platforms, where channels are half-buried in substrates, fins are grown on the surface of substrates, and in such a structure, high-cost and complex suspended devices are unnecessary; instead, all the devices are wrapped over the fin. Traditional PICs based on SOI have 2D devices while 3D platforms, while this construction has "2D-lized" platforms, and "3D-lized" devices, which enables planar process to make most of the fabrication work, and thus, make cost more controllable.

With the knowledge of the fin-structure channels, it's time to introduce the III-Nitride FSML in this research. The most obvious application of this laser is the light source in fin-structure photonic integrated circuit. From the first product of commercialized parallel link of HP company to recent efforts for Terabus, parallel links went from separated modules to integrated modules, which have smaller volume and lower cost. However, till recent days, the footprint of a single VCSEL requires the area of decades of um^2 typically, which is a huge object compared with sub-micro scale electrical devices. Because of that, it is desirable to shrink the footprint of devices dramatically, and that can be achieved by changing the 2D device to 3D fin-structure device. Besides, the size of fibers or waveguides applied in

traditional parallel links are large in order to support infare (850nm typically). To make channels smaller, one effective way to do is to apply shorter wavelength such as blue or violet light. For single mode propagation, waveguide for that wavelength can be as small as decades of nanometers. Figure 10 is how fin-structure parallel links look like in integrated circuit.

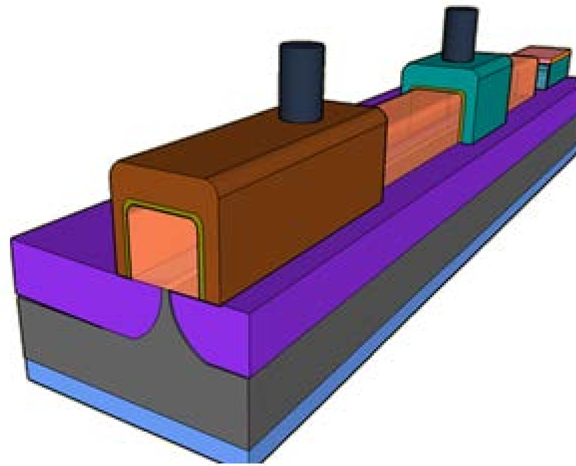

Figure 10. Parallel links based on Fin-Structure Micro-Laser

In figure 10, the box at the far end is FSML. Light generated from there propagates along the waveguide and reaches semiconductor optical amplifier (SOA) in the middle before being received by the photodetector, which convert the light signals to electric signals. In this blueprint, couplers, lens array and flip-chip mounted IC are removed, and the complexity of optical-to-electric part is reduced effectively, and because of the maturity of Fin-FET, the FSML, technologically speaking, cannot be too much expensive.

1.3. Material Systems

1.3.1. Long wavelength VCSELs

Almost all commercialized VCSELs are long wavelength VCSELs, and that is caused by the following reasons: first, VCSELs based on narrow bandgap semiconductor materials, such as InP and GaAs, are matured; second, in long distance transmission, long wavelength light is more compatible for many fibers and substrate materials for less power absorption, thus 850nm light is fiber-based standard in many applications; third, in order to achieve single mode propagation, fibers or waveguides support short wavelength have to be made extremely thin, which increases the cost and difficulties in channel fabrication; fourth, Si, which are widely applied in integrated circuit, are transparent for long wavelength light, which brings about less power loss; fifth, when red surface emitting laser were created in 1980s, researches on blue light LED based on GaN were still at very early stages, so, needless to say, it takes time for III-nitride VCSELs to be accepted by the market; and last but not least, materials of long wavelength VCSELS suffer from smaller lattice mismatch with cheap silicon substrate comparing with blue light materials such as GaN. Because of these facts and considerations, red or infare VCSELs are applied first. Commercialized wavelength includes (a)850nm and (b)980nm; material systems for these two groups are introduced below.

(a) 850nm VCSELs

GaAs/AlGaAs can be regarded as the most successful VCSEL material, and it is the

best choice for 850nm multi quantum well VCSEL so far. More than 20GHz bandwidth was achieved based on this material by K. L. Lear et al., [19] and this record has not been updated.

The second material system that is worthwhile to pay attention to is InGaAs/AlGaAs, C. Lei et. Al., found out, in 2002, that if the quantum well material GaAs was doped with a small fraction of Indium, the material gain can be doubled [20]. Till now, the data rate of 32Gbit/s and 39Gbit/s were demonstrated in InGaAs/AlGaAs devices [21] [22].

(b) 980nm VCSELs

980nm is another commonly applied wavelength in VCSEL data transmission, which can be achieved by aluminum-free InGaAs/GaAs system. 980nm wavelength is transparent in GaAs substrates, so this kind of VCSEL is potential to be used in bottom emission VCSEL.

The highest modulation current efficiency factor (MCEF) of MQW InGaAs/GaAs VCSEL with the wavelength of 980nm is 16.8GHz/mA$^{1/2}$, and it was achieved by K. L. Lear et. al., in 1996 [23]. The dimension of that device is only 9 um^2, with the threshold current of 0.37mA, and DQE of 45%.

Another effort also focuses on InAs quantum dot, which provide larger differential gain and improved temperature insensitivity. In the report of reference [24], when temperature changes from 25°C to 85 °C, the threshold only changes from 0.29mA to 0.16mA.

There are also longer wavelength VCSEL based on GaAs and its alloy and InP. Generally, these technologies are matured and even ready for commercialization. However, for shorter wavelength, the progress is much slower since the material and the corresponding

suitable substrate are limited.

1.3.2. III-Nitride VCSELs

Lasers based on III-Nitride material are much less developed than GaInAsP/InP and AlGaAs/GaAs counterparts. Different from the other two groups, the lasing behavior of III-Nitride VCSELs is dominantly under optical pumping condition, so it is faced to three difficulties: first, there is almost no proper substrate for GaN lasers. Growing on improper substrate, GaN contains a lot of defects, which dramatically reduces device performance, and particularly, leads to short laser lifetime. Second, p-type doping is limited even though Mg dopants are often applied. Usually, the p-doping density is lower than $10^{18}/cm^3$ and is significantly lower than n-doping. What's more, lattice mismatch between AlN and GaN makes high-quality and high-reflective DBRs difficult, which are likely to be used as the bottom DBRs. Because of these drawbacks, III-Nitride VCSELs can hardly make breakthrough.

Even though we have no effective way to solve p-doping problem in this research, we put forwards a III-nitride micro-laser with fin-structure which is potential to break the limitations on substrates and defects.

References

[1] Graham William Read, Igor Pavlovich Marko, Nadir Hossain, Stephen John Sweeney, “Physical properties and characteristics of III-V lasers on silicon”, IEEE Journal of Selected Topics in Quantum Electronics. **21** (6), November/ December 2015, Article Sequence Number: 1502208.

[2] John T. Leonard, “III-Nitride Vertical-Cavity Surface-Emitting Lasers”, Dissertation (March 2016), University of California, Santa Barbara.

[3] Kenichi Iga, “Surface-Emitting Laser—Its Birth and Generation of New Optoelectronics Field”, IEEE Journal of Selected Topics in Quantum Electronics, **6** (6), November/December 2000.

[4] K. Iga, S. Ishikawa, S. Ohkouchi, and T. Nishimura, “Room-Temperature Pulsed Oscillation of GaAlAs/GaAs Surface Emitting Injection Laser”, Appl. Phys. Lett. **45**, 348 (1984).

[5] Seiji Uchiyama, Enichi Iga, “GaInAsPAnP Surface Emitting Injection Laser with a Ring Electrode”, IEEE Journal of Quantum Electronics, Vol. QE-20, No. 10, October 1984.

[6] Kenichi Iga, Seiji Uchiyama, “GalnAsP/lnP Surface-Emitting Laser Diode”, Optical and Quantum Electronics **18** (1986) 403-422.

[7] K. Iga, S. Kinoshita, F. Koyama, “Microcavity GaAlAs/GaAs Surface-Emitting Laser with I_{th} = 6mA”, Electronics Letters, **23**(3), 29th January 1987.

[8] A. Chailertvanitkul, K. Iga, K. Moriki, “GalnAsP/lnP Surface-Emitting Laser (X = 1-4 µm. 77 K) with Heteromultilayer Bragg Reflector”, Electronics Letters **21**(7): 303 - 304 · March 28 1985.

[9] S. Boussakta, A. G. J. Holt, “Vertical Cavity Surface-Emitting Laser with an AlGaAs/AlAs Bragg Reflector”, Electronics Letters **24**(15): 928 - 929, 21st July 1988.

[10] Terence Edward Sale, “Vertical Cavity Surface Emitting Lasers”, Thesis (September), University of Sheffield (1993).

[11] Isamu Akasaki and Hiroshi Amano, “Widegap Column-Ill Nitride Semiconductors for UV/Blue Light Emitting Devices”, J. Electrochem. Soc., **141**(8), 2266-2271, August 1994.

[12] Shuji Nakamura, Takashi Mukai, and Masayuki Senoh, “Candela-class high-brightness InGaN/AlGaN double-heterostructure blue-light emitting diodes”, Appl. Phys. Lett. **64**, 1687 (1994).

[13] Shuji Nakamura, Masayuki Senoh, Shin-ichi Nagahama, et, al., “High-Power, Long-Lifetime InGaN/GaN/AlGaN-Based Laser Diodes Grown on Pure GaN Substrates”, Jpn. J. Appl. Phys. Vol. 37 (1998) pp. L 309–L 312, Part 2, No. 3B, 15 March 1998.

[14] Meryem Primmer, “An Introduction to Fibre Channel”, Hewlett-Packard Journal, October 1996, Article 11.

[15] Prasad M and Dr. U B Mahadevaswamy, “Comparative Study of MOSFET, CMOS and FINFET: A Review”, Grenze ID: 02, ICCTEST.2017.1.62.

[16] R. Michalzik, G. Giaretta, K.W. Goossen, J.A.Walker,M.C. Nuss, “40 Gb/s coarse WDM data transmission with 825nm wavelength VCSELs over 310m of high-performance multimode fiber”, in proceedings of 26th European Conference on Optical Communications, ECOC, vol. 4 Munich, Sept, 2000, pp 33-34.

[17] R.R. Patel, S.W. Bond, M.D. Pocha, et, al., “Multiwavelength parallel optical interconnects for massively parallel processing”, IEEE Journal of Selected Topics in Quantum Electronics. **9**(2), pp 657–666, 27 October 2003.

[18] Martijn J. R. Heck, Jared F. Bauters, Student Member, et, al., “Hybrid Silicon Photonic Integrated Circuit Technology”, IEEE Journal of Selected Topics in Quantum Electronics, **19**(4), July/August 2013**,** Article Sequence Number: 6100117.

[19] K.L. Lear, V.M. Hietala, H.Q. Hou, J. Banas, B.E. Hammons, J. Zolper, S.P. Kilcoyne, “Small and large signal modulation of 850 nm oxide-confined vertical-cavity surface-emitting lasers”, in Conference on Lasers and Electro-Optics, 1997, DOI: 10.1109/CLEO.1997.602456.

[20] T. Aggerstam, R.M.V. Würtemberg, C. Runnström, E. Choumas, “Large aperture 850nm oxide confined VCSELs for 10Gb/s data communication”, Proc. SPIE 4649, Vertical-Cavity Surface-Emitting Laser VI, (4 June 2002); DOI: 10.1117/12.469244.

[21] P. Westbergh, J.S. Gustavsson, A. Haglund, A. Larsson, F. Hopfer, G. Fiol, D. Bimberg and A. Joel, “32 Gbit/s multimode fibre transmission using high-speed, low current density 850 nm VCSEL”, Electronics Letters, **45** (7), pp 366 – 368, 26th March 2009.

[22] P. Westbergh, J.S. Gustavsson, B. Kogel, A. Haglund, A. Larsson, A. Mutig, A. Nadtochiy, D. Bimberg and A. Joel, “40 Gbit/s error-free operation of oxide-confined 850 nm VCSEL”, Electronics Letters, **46**(14), pp 1014 – 1016, 12 July 2010.

[23] K.L. Lear, A. Mar, K.D. Choquette, S.P. Kilcoyne, R.P. Schneider Jr., K.M. Geib, “Highfrequency modulation of oxide-confined vertical cavity surface emitting lasers”. Electronics Letters. **32**(5), pp 457 – 458, 29 February 1996.

[24] F. Hopfer, A. Mutig, G. Fiol, M. Kuntz, S.S. Mikhrin, et, al., “20 Gb/s direct modulation of 980nm VCSELs based on submonolayer deposition of quantum dots”, Proc. SPIE 6350, Workshop on Optical Components for Broadband Communication, 635003 (6 July 2006); DOI: 10.1117/12.693006

[25] Rainer Michalzik, “VCSELs Fundamentals, Technology and Applications of Vertical-Cavity Surface-Emitting Lasers” (Springer-Verlag, 2012).

[26] Bo-Rong Huang, Fan-Hsuan Meng, Ya-Chin King, and Chrong Jung Lin, “Investigation of parasitic resistance and capacitance effects in nanoscaled FinFETs and their impact on static random-access memory cells”, Japanese Journal

of Applied Physics 56, 04CD11 (2017).

[27] Andreas C. Cangellaris, "The Interconnect Bottleneck in Multi-GHz Processors; New Opportunities for Hybrid Electrical/Optical Solutions", Massively Parallel Processing, 1998. Proceedings. Fifth International Conference on, pp. 96–103, 1998.

[28] Caro Bayo, Miguel Ángel, "Theory of elasticity and electric polarization effects in the group-III nitrides", PhD Thesis (2013), University College Cork.

2. FSML DESIGN

In this chapter, we are going to focus on the design of components of FSML. The basic and unquantized model will be figured out first, followed by the design and quantization of each part. FSML as a whole is a symmetric structure, consisted of LEDs, DBRs, a waveguide, and a cavity, which satisfy standing wave condition. The primary model is presented in figure 14.

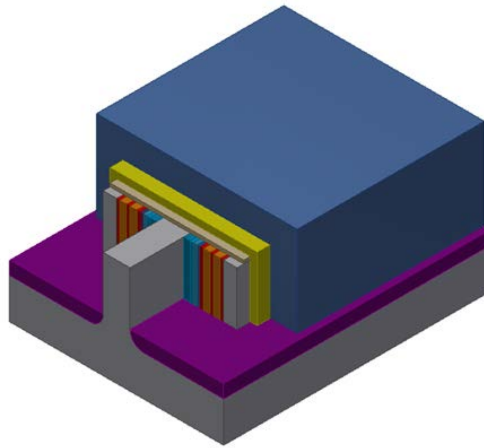

Figure 11. 3-D structure of FSML

The FSML shown in figure 11 is a laser with 3 pairs of quantum wells (QWs, each side of the fin has three quantum wells), which is named as three-QW FSML. The fin in the center is c-plane GaN, grown by epitaxy, which plays three roles in this device: (1) it is the supporting part of the whole device; it is grown first, followed by other layers one after another; (2) it is the electron-transporting layer where electrons injected from its bottom and drift into active regions of the laser; (3) its extended part is waveguide that is loss-freely coupled with Lasers. In order to achieve all the functions required above, this part, wrapped

in the laser, should be highly doped, and luckily, the n-type doping of GaN with high concentration is achievable. Depending on the fin, two LEDs can be deposited on the two edges by epitaxy. In order to prevent the growth on top of the fin, a blocking layer should be deposited above the fin before the growth of LED. To match the n-type fin, the n-region of each LED, which is followed by active regions and the p-region, should be adjacent to the fin. Then an insulation layer is deposited above; after that, the whole structure needs to be wrapped by p contact with the material of ITO in this research. The structure so far is a fin-structure symmetric LED shown in figure 12, and if it is wrapped with highly reflected DBRs (blue region in figure 11), it can become a FSML.

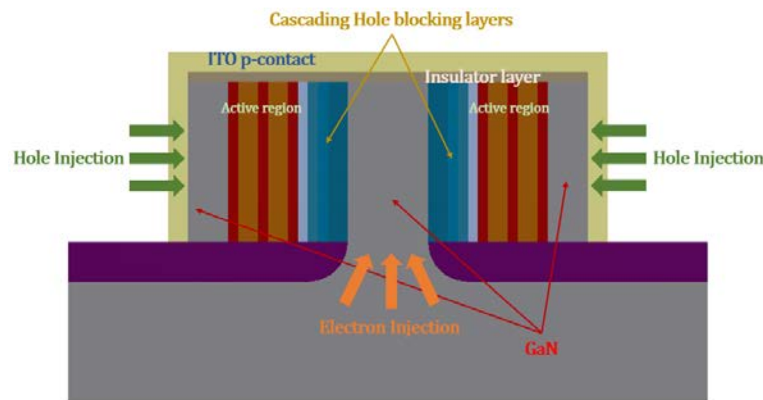

Figure 12. Cross-section of fin-structure LED

Figure 15 also presents how does this device work. Since ITO is the p-contact layer, it provides holes for the device; therefore, holes enter the device through the walls on two sides. Electrons are injected from the bottom of the fin, which is the n contact. Optical transition occurs at the active region, and the emitting direction is out-of-plane direction, which is similar to EELD.

2.1. LED Designs

We started our work from fin-LED design, and analyzed the performance of LEDs with different numbers of quantum wells. Fin-LED is applied in FSML as a “pumping source”, and its emission intensity, to some degree, determines the output power of the laser. By manipulating the band structure, holes and electrons density in QWs match with each other so that the Internal Quantum Efficiency reaches its optimum. Leakage of current can be reduced by adding blocking layers so that the spectrum is dominantly contributed by QWs and the energy loss is suppressed. The performance of an LED can be judged by JV curve, Internal Quantum Efficiency, droop effect, carrier matching in QWs, leakage and spectrum, and our research is started from the 1D simulation of LED model.

2.1.1. 1-D simulation

1D simulation is helpful for understanding the band structure of an LED and the carrier distribution, especially, carriers in QWs. Usually, because of the unequal carrier mobility of holes and electrons, the density of holes and electrons are unmatched, which lead to the dropping down of emission rate. Hole-injection is a large problem for III-Nitride LED design, and the leakage of hole current needs to be suppressed.

Necessary parameters for LED design is listed in table 2, and the band diagram of materials can be determined based on the following equations [1]:

$$E_{g,InxGa1-xN} = xE_{g,InN} + (1-x)E_{g,GaN} - 1.43x(1-x)$$

$$E_{g,AlxGa1-xN} = xE_{g,AlN} + (1-x)E_{g,GaN} - 1.3x(1-x)$$

Table 2. Necessary parameters for LED design

Parameter	Value	reference
$E_{g,InN}(eV)$	0.77	[1]
$E_{g,GaN}(eV)$	3.425	
$E_{g,AlN}(eV)$	6.28	
Auger coefficient (cm^6/s)	5e-33	[2]
SHR $(1/s)$	1.6e7	
InN electron affinity (eV)	5.7	[1]
GaN electron affinity (eV)	4.1	
AlN electron affinity (eV)	1.9	
Hole mobility (cm^2/Vs)	22	[3]
Electron mobility (cm^2/Vs)	940	
Band offset ratio	0.3	[1]

Here I present three devices with the number of QWs of one, two, three, respectively. In these devices, cascading hole blocking barriers (HBL) made of AlGaN were inserted between active region and n-transporting layers. For multi-QW devices, the band gap of barriers need to be adjusted to make carrier-density matching in QWs. Eventually, the quantified LED structures are presented in table 3.

Table 3. Quantified LED design for 1-D simulation

One QW Device			Two QW Device			Three QW Device		
Material	Dimension (nm)	Doping(cm^{-3})	Material	Dimension (nm)	Doping(cm^{-3})	Material	Dimension (nm)	Doping(cm^{-3})
n-GaN	70	1e18	n-GaN	55	1e18	n-GaN	40	1e18
n-$Al_{0.16}Ga_{0.84}N$	30	1e18	n-$Al_{0.16}Ga_{0.84}N$	30	1e18	n-$Al_{0.16}Ga_{0.84}N$	30	1e18
n-$Al_{0.12}Ga_{0.88}N$	4	1e18	n-$Al_{0.12}Ga_{0.88}N$	4	1e18	n-$Al_{0.12}Ga_{0.88}N$	4	1e18
$Al_{0.08}Ga_{0.92}N$	5	0	$Al_{0.08}Ga_{0.92}N$	5	0	$Al_{0.08}Ga_{0.92}N$	5	0
$Al_{0.04}Ga_{0.96}N$	5	0	$Al_{0.04}Ga_{0.96}N$	5	0	$Al_{0.04}Ga_{0.96}N$	5	0
$In_{0.17}Ga_{0.83}N$	5	0	$In_{0.17}Ga_{0.83}N$	5	0	$In_{0.17}Ga_{0.83}N$	5	0
GaN	20	0	$In_{0.08}Ga_{0.92}N$	10	0	$In_{0.10}Ga_{0.90}N$	10	0
p-GaN	55	1e17	$In_{0.17}Ga_{0.83}N$	5	0	$In_{0.17}Ga_{0.83}N$	5	0
			GaN	20	0	$In_{0.10}Ga_{0.90}N$	10	0
			p-GaN	55	1e17	$In_{0.17}Ga_{0.83}N$	5	0
						GaN	20	0
						p-GaN	55	1e17

Simulation of these three devices has been carried out on COMSOL Multiphysics, and the results of band structures and carrier densities, which are instructive for 2D model later, are presented in figure 13.

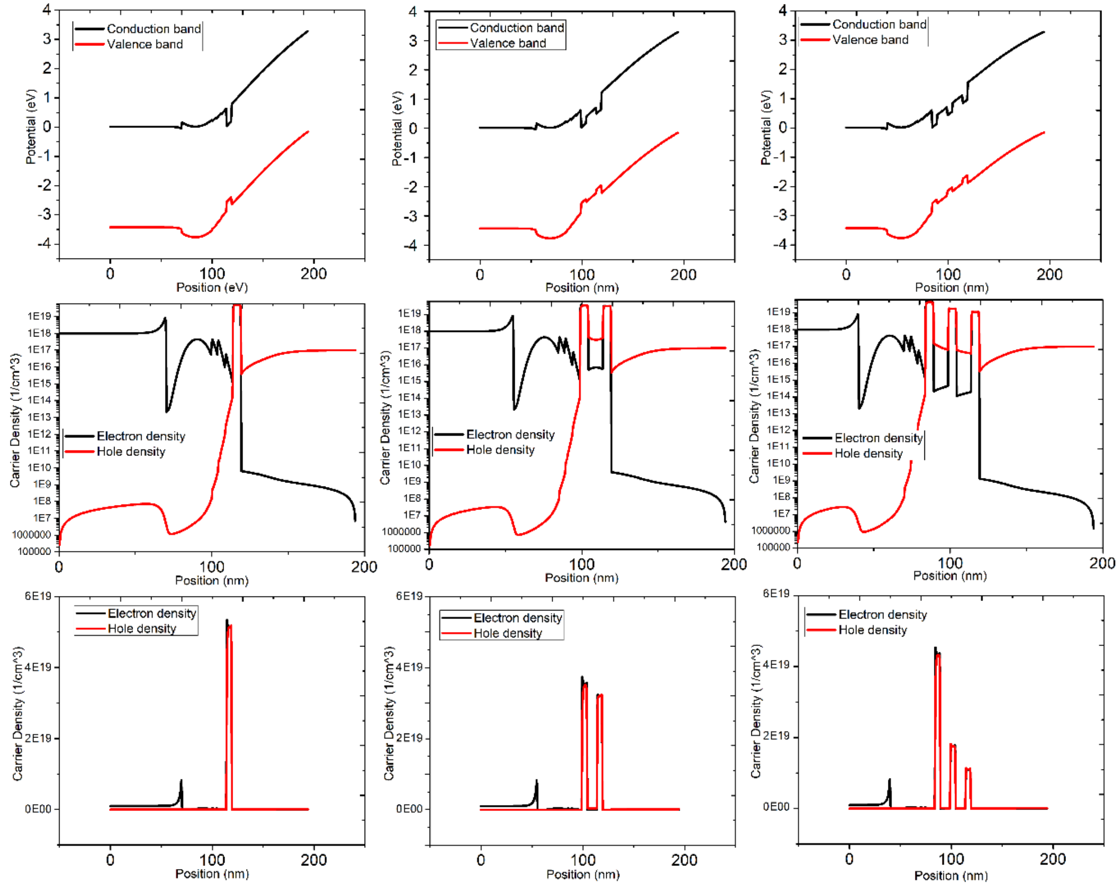

Figure 13. Band structure and carrier distribution of one/two/three-QW LEDs. (a), (b), (c) one-QW band structure and carrier distribution in log and original scale; (d), (e), (f) two-QW band structure and carrier distribution in log and original scale; (g), (h), (i) three-QW band structure and carrier distribution in log and original scale;

The measurement of figure 13 (a, b, c) is under the condition of 0V; at zero bias, the p region is bended up because of the relatively low doping concentration. The measurement of figure 13(d, e, f, g, h, i) is in the current bias of $1000A/cm^2$, and the carrier distribution in QWs matches well. Therefore, we can move on to the 2D simulation.

2.1.2. 2-D simulation

2D models are expanded directly from the corresponding 1D models. Firstly, the half cross section can be built based on 1D models by adding another dimension; next, mirror-flip the half cross section with the symmetric axis of the fin to get the 2D cross section model; finally, move the n-contact to the bottom of the fin so that the geometric structure and boundary condition setting are finished. We name the device after one/two/three-QW 1D model directly, even though the actual number of QWs should be doubled. Figure 14 presents some of the features of these devices according to the COMSOL simulation.

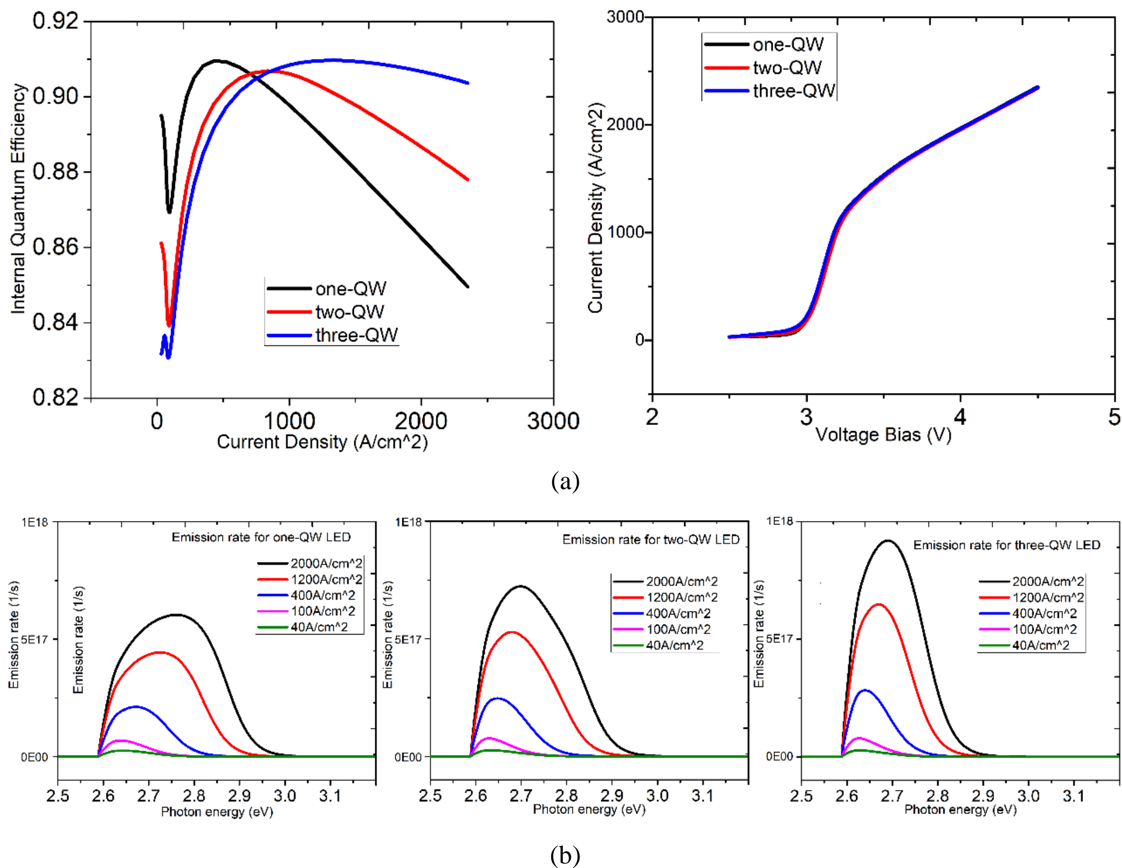

Figure 14. General performances of LEDs (a) JV curves and IQE curves for one/two/three-QW LED (b) Emission power (W) vs. Frequency (Hz) for one/two/three-QW LEDs (from left to right) in different current bias.

The intensity (unit: 1/s) is spontaneous emission in quantum wells. However, considering the power absorption, scattering and reflection, the actual output power is depended on External quantum efficiency and should be much smaller than this. According to the IQE curve presented in Figure 14 (a), the drooping effect is delayed when the number of QWs increases: on one-QW devices, droop effect shows up as early as 450A/cm^2, while for three-QW devices, it is delayed to 1400A/cm^2. Figure 14 (b) is the spectrum in different current bias. An obvious observation is that as the number of QWs increases, the emission intensity goes larger; and as the current increases, the spectrum shows "blue-shift effect", and that is because injected carriers in QWs occupy higher energy level when the current bias is larger.

So far, the LED simulation is finished. Beyond the electric study on LEDs, optical study on DBRs, cavities are also carried out in the following.

2.2. Distributed Bragg Reflectors (DBRs) Designs

DBRs are high-reflection mirrors consisted of repeated two-layer pairs (DBR periods) with the thickness of 1/4 wavelength ($\lambda/4n_{real}$). The difference on refractive index of the two layers and the number of periods determine the reflection rate: if the difference is large, high-reflection can be achieved with small number of pairs and vice versa. In order to confine the light power, the real part of refractive index of DBR materials should be smaller than the LED core, and the imaginary part should be as small as possible in order to reduce power absorption.

2.2.1. The Transmission Matrix Method

Transmission Matrix Method (TMM) is a simple description of the interaction of electromagnetic wave and materials. Based on this method, we can calculate the reflectance, transmission, and absorption spectra, so it is a very useful tool for us to determine the design of DBRs.

Light propagation in bulk material, in transmission matrix, can be described as

$$T_{bulk} = \begin{pmatrix} e^{i\beta L} & 0 \\ 0 & e^{-i\beta L} \end{pmatrix}$$

β and L are propagation constant and distance, respectively, and β is defined as

$$\beta = \frac{2\pi n}{\lambda}$$

where n in this expression is a complex number:

$$\mathrm{n} = n_{real} - jk$$

n_{real} is reflective index and k is extinction coefficient, which determines the absorption coefficient of materials.

$$\alpha = \frac{4\pi k}{\lambda}$$

Light is very sensitive for the change of reflective index, so when the beam hits the interface of layer 1 and layer 2, it will experience transmission and reflection, which can be quantitively described by transmission coefficient and reflection coefficient respectively:

$$t_{12} = \sqrt{1 - \left(\frac{n_2 - n_1}{n_2 + n_1}\right)\left(\frac{n_2 - n_1}{n_2 + n_1}\right)^*}$$

$$r_{12} = \frac{n_2 - n_1}{n_2 + n_1}$$

where "*" is the sign of complex conjugate. Based on these two coefficients, we can

define the transmission at the interface of two materials:

$$T_{12} = \frac{1}{r_{12}}\begin{pmatrix} 1 & r_{12} \\ r_{12} & t_{12}^2 + r_{12}r_{12}^* \end{pmatrix}.$$

Now, let's consider something more complex; in the situation of laser, light emission from p-type GaN goes through ITO, DBRs, and eventually, goes into air. So, the total transmission matrix can be described as:

$$T_{total} = T_{12}^{GaN/ITO} T_{bulk}^{ITO} T_{12}^{ITO/Si_3N_4} \left(T_{bulk}^{Si_3N_4} T_{12}^{\frac{Si_3N_4}{SiO_2}} T_{bulk}^{SiO_2} T_{12}^{\frac{SiO_2}{Si_3N_4}} \right)^{q-1} T_{bulk}^{Si_3N_4} T_{12}^{Si_3N_4/SiO_2} T_{bulk}^{SiO_2} T_{12}^{SiO_2/air}$$

where q is the number of periods of DBRs. The reflected/transmitted power, based on T_{total} can be expressed as:

$$\mathrm{R} = \frac{T_{Total}(2,1)T_{Total}(2,1)^*}{T_{Total}(1,1)T_{Total}(1,1)^*}$$

$$\mathrm{T} = \sqrt{1 - \frac{T_{Total}(2,1)T_{Total}(2,1)^*}{T_{Total}(1,1)T_{Total}(1,1)^*}}$$

where the indices in brackets are the coordinates of the matrix elements.

2.2.2. Reflection Spectra

With the knowledge of this, MATLAB code can be made to generate reflectance spectra of DBRs. Assume our target wavelength is 461.22nm, which is corresponding to the peak of LED spectrum, so the thickness of Si_3N_4 and SiO_2 should be 58nm and 79 nm respectively. Figure 15 is the reflectance spectra of 8/12/16 DBRs periods.

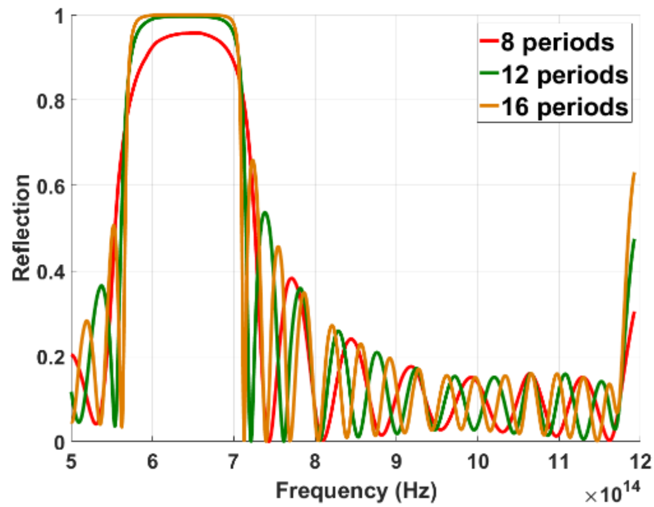

Figure 15. Reflectance spectra of DBRs

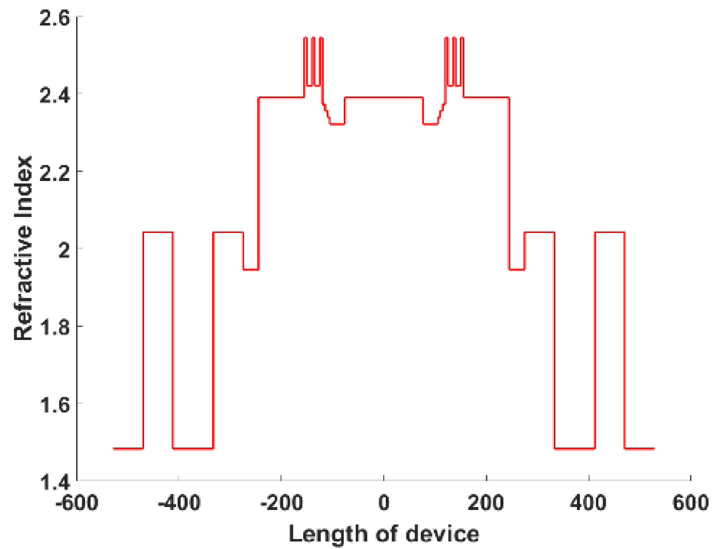

Figure 16. Reflective index of materials

The reflectance of DBRs should be as large as possible in order to reduce the energy loss of the laser, which has great impact on the threshold gain of laser.

Assume the reflectance of DBR is R, and the cavity length is L. The power loss caused by the DBR for each trip (propagate from the right to the left and get reflected) can be

converted to *Loss/m* with the method:

$$e^{-\alpha L} = R$$

where L is the cavity length in the unit of "m", and $\alpha = -\frac{lnR}{L}$.

2.3. Cavity Designs

The function of the cavity in a laser device is to "reshape" the spectrum of LED or selectively amplify the power of target wavelength and extinct others. The principle of cavity design is that the cavity length must satisfy standing wave condition for the target wavelength. If the reflective index of materials in cavity is uniform, the cavity length is very easy to be calculated. However, the problem for us is much more complex: the reflective index distribution in semiconductor laser is not uniform; it can be presented as figure 16. Therefore, the main challenge in device quantization is the cavity design.

Although the standing wave condition for our target wavelength is difficult to be solved by manual calculation, section 2.3.1. describes how to figure out it with COMSOL, and 2.3.2 quantitively shows the influence of absorption of gain materials.

2.3.1. Standing wave condition

Basically, in order to satisfy the standing wave condition, the cavity length can be calculated with the equation:

$$\frac{1}{\lambda_q} = \frac{q}{2nL}$$

where q is an arbitrary natural number which means mode. If the mode number is large, the cavity length L is large, and vice versa. However, for the situation of our device, the n is not

a constant, yet we assume $n = n_{GaN}$ and "q" is equal to 6, so that we can find out the approximate cavity length L. L subtracts the length of double-LED dimension (which has been defined in the section of 2.1.) and double-ITO thickness (assume 30nm for each), and we can get the approximate width of the fin.

Actually, the refractive index of materials in cavity are not ideally equal to n_{GaN}. For ITO, we had learned that in section 2.2.2, and the reflective index of III-Nitride alloy can be estimated with the equation [1] of:

$$n_{Al_xGa_{1-x}N} = n_{GaN} - 0.43x$$

$$n_{In_xGa_{1-x}N} = n_{GaN} + 0.91x$$

With the knowledge of LED dimension, ITO thickness, approximate fin-width, and DBR, and the complex refractive index of all layers, we can build a resonant cavity model, and predictably, the resonance frequency obtained from that model is not our target frequency, but it cannot be far away from the target because most of the region in the cavity is GaN and its alloy, and by adjusting the fin size one nanometer by one nanometer, we can shift the resonant frequency gradually to approach the target, and foreseeably, the desirable fin size will be figured out, and once we do that, the size of the laser can be quantized, and the results presented in table 4. This process is carried out on one-QW device, so that its cavity length should be optimal. Theoretically, we need to do the same process to get the optimal cavity length of two/three-QW laser, however, in order to compare the influence of number of QWs only, the influence of cavity length should be eliminated; therefore, the

cavity length determined by one-QW device is fixed, and also applied to two/three-QW device.

2.3.2. Absorption of III-Nitride Materials in Cavity

The consideration of internal absorption of cavity is unnecessary in cavity design because it has no influence on the resonant frequency. But the absorption has actual influence on the cavity performance, especially quality factor. In this section, we analyzed the cavity performance with extinction coefficient. The models we applied are models in table 4.

Extinction coefficient of common materials can be downloaded from https://refractiveindex.info/, and as for $In_xGa_{1-x}N$ alloy, the absorption coefficient can be derived from reference [4], [6], [7]. And at the range of LED spectrum $\kappa_{AlGaN} = 0$ [5].

Q factor at resonance frequency (one of the eigenvalue frequencies) is a useful tool to measure the performance of a laser cavity. In definition:

$$\mathrm{Q} = \frac{2\pi f_0 E}{P}$$

where f_0 is the resonant frequency; E and P are the stored energy in cavity and power dissipated respectively. In real measurement, wavelength of light source is usually changed continuously to read the resonant frequency and full width at the half maxima, so that Q factor can be calculated with the formula:

$$\mathrm{Q} = \frac{f}{\Delta f}$$

In COMSOL simulation, resonant frequency and Q factor can be obtained by solving

eigenvalue equation. Figure 17 cavity Q factors with different periods of DBRs.

Table 4. Laser design, one/two/three-QW laser is named after the number of QWs of half device cross section, so the actual number of QWs in device should be doubled; n is the number of DBR periods, which leads to large reflectance.

One-QW Laser			Two-QW Laser			Three-QW Laser		
Material	Dimension (nm)	Doping(cm^{-3})	Material	Dimension (nm)	Doping(cm-3)	Material	Dimension (nm)	Doping(cm-3)
SiO_2/Si_3N_4	$\times n$		SiO_2/Si_3N_4	$\times n$		SiO_2/Si_3N_4	$\times n$	
ITO	30	0	ITO	30	0	ITO	30	0
p-GaN	50	1e17	p-GaN	50	1e17	p-GaN	50	1e17
GaN	25	0	GaN	25	0	GaN	25	0
$In_{0.17}Ga_{0.83}N$	5	0	$In_{0.17}Ga_{0.83}N$	5	0	$In_{0.17}Ga_{0.83}N$	5	0
$Al_{0.04}Ga_{0.96}N$	5	0	$In_{0.08}Ga_{0.92}N$	10	0	$In_{0.10}Ga_{0.90}N$	10	0
$Al_{0.08}Ga_{0.92}N$	5	0	$In_{0.17}Ga_{0.83}N$	5	0	$In_{0.17}Ga_{0.83}N$	5	0
n-$Al_{0.12}Ga_{0.88}N$	4	1e18	$Al_{0.04}Ga_{0.96}N$	5	0	$In_{0.10}Ga_{0.90}N$	10	0
n-$Al_{0.16}Ga_{0.84}N$	30	1e18	$Al_{0.08}Ga_{0.92}N$	5	0	$In_{0.17}Ga_{0.83}N$	5	0
n-GaN	26	1e18	n-$Al_{0.12}Ga_{0.88}N$	4	1e18	$Al_{0.04}Ga_{0.96}N$	5	0
n-GaN	286	1e19	n-$Al_{0.16}Ga_{0.84}N$	30	1e18	$Al_{0.08}Ga_{0.92}N$	5	0
n-GaN	26	1e18	n-GaN	26	1e18	n-$Al_{0.12}Ga_{0.88}N$	4	1e18
n-$Al_{0.16}Ga_{0.84}N$	30	1e18	n-GaN	256	1e19	n-$Al_{0.16}Ga_{0.84}N$	30	1e18
n-$Al_{0.12}Ga_{0.88}N$	4	1e18	n-GaN	26	1e18	n-GaN	26	1e18
$Al_{0.08}Ga_{0.92}N$	5	0	n-$Al_{0.16}Ga_{0.84}N$	30	1e18	n-GaN	226	1e19
$Al_{0.04}Ga_{0.96}N$	5	0	n-$Al_{0.12}Ga_{0.88}N$	4	1e18	n-GaN	26	1e18
$In_{0.17}Ga_{0.83}N$	5	0	$Al_{0.08}Ga_{0.92}N$	5	0	n-$Al_{0.16}Ga_{0.84}N$	30	1e18
GaN	25	0	$Al_{0.04}Ga_{0.96}N$	5	0	n-$Al_{0.12}Ga_{0.88}N$	4	1e18
p-GaN	50	1e17	$In_{0.17}Ga_{0.83}N$	5	0	$Al_{0.08}Ga_{0.92}N$	5	0
ITO	30	0	$In_{0.08}Ga_{0.92}N$	10	0	$Al_{0.04}Ga_{0.96}N$	5	0
Si_3N_4/SiO_2	$\times n$		$In_{0.17}Ga_{0.83}N$	5	0	$In_{0.17}Ga_{0.83}N$	5	0
			GaN	25	0	$In_{0.10}Ga_{0.90}N$	10	0
			p-GaN	50	1e17	$In_{0.17}Ga_{0.83}N$	5	0
			ITO	30	0	$In_{0.10}Ga_{0.90}N$	10	0
			Si_3N_4/SiO_2	$\times n$		$In_{0.17}Ga_{0.83}N$	5	0
						GaN	25	0
						p-GaN	50	1e17
						ITO	30	0
						Si_3N_4/SiO_2	$\times n$	

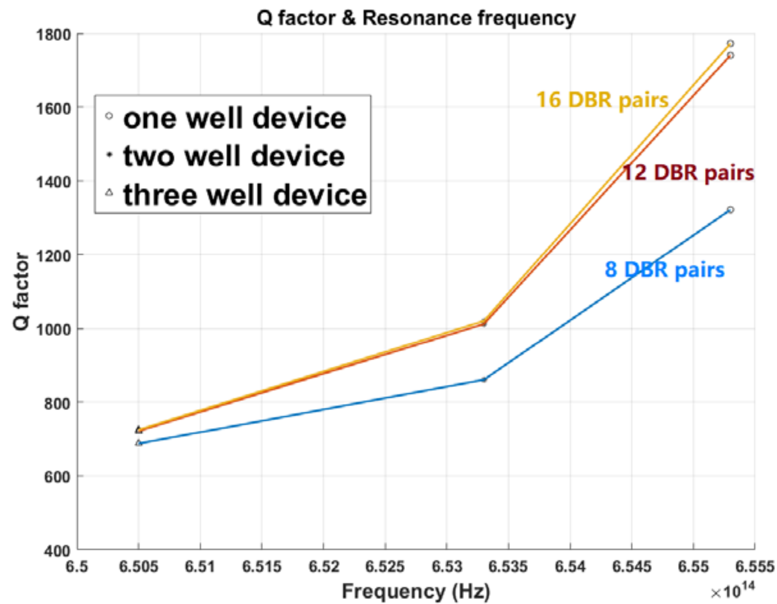

Figure 17. Q-factor and Resonance frequency

According to figure 17, we can learn that one-QW laser has the best design among these three devices. As mentioned before, we fixed the cavity length for the three lasers; however, for pursuing the optimal performance, the cavity length should be calculated individually since the distribution of reflective index varies with alloy concentration.

2.4. Waveguide Simulation

The purpose of this section is to provide a method to measure the quality of the fin as the channel of light signal. As a supporting structure and carrier transporting layer in laser, the fin design is successful; yet as a waveguide, signal mode condition should be taken into account.

In order to estimate the mode condition of the waveguide, we first made a 1D

simulation for planar waveguide model to measure the number of mode that can be contained in the waveguide, and then a 3D model of rib waveguide has been done to see the energy distribution in the fin.

2.4.1. 1-D Model for Planer Waveguide Simulation

Planar waveguide model is the simplest model to calculate the modes supported in waveguide by solving eigenvalue equation. Firstly, we can assume three variables:

$$\mathrm{q} = \sqrt{\beta^2 - k_0^2 n_1^2}$$
$$\mathrm{h} = \sqrt{k_0^2 n_2^2 - \beta^2}$$
$$\mathrm{p} = \sqrt{\beta^2 - k_0^2 n_3^2}$$

where β is propagation constant, k_0 is wavenumber, and $n_{1/2/3}$ is the refractive index of corresponding materials. For waveguide, n_2 must be the largest among n_1, n_2, n_3.

For TE polarized wave, the eigenvalue equation should be like:

$$\tan(\mathrm{hd}) = \frac{q+p}{h - \frac{qp}{h}}$$

where "d" is the width of waveguide. For more special condition, if the waveguide is symmetric ($n_1 = n_3$), eigenvalue equation can be simplified as:

$$\tan(\mathrm{hd}/2) = \begin{cases} \frac{q}{h} & \text{for even modes} \\ -\frac{h}{q} & \text{for odd modes} \end{cases}$$

For TM polarized wave, the eigenvalue equation is:

$$\tan(\mathrm{hd}) = \frac{\frac{n_2^2}{n_3^2} p + \frac{n_2^2}{n_1^2} q}{h - \left(\frac{n_2^2}{n_1 n_3}\right)^2 \left(\frac{qp}{h}\right)}$$

and for symmetric situation:

$$\tan\left(\frac{\text{hd}}{2}\right) = \begin{cases} \left(\frac{n_2}{n_1}\right)^2 \frac{q}{h} & \text{for even modes} \\ -\left(\frac{n_1}{n_2}\right)^2 \frac{h}{q} & \text{for odd modes} \end{cases}$$

In condition, the GaN waveguide is sandwiched by air, the frequency of the input wave is corresponded to resonance frequency in section 2.3, and we considered both TE mode and TM mode. Figure 18 presents the modes that is supported by waveguide in planar model.

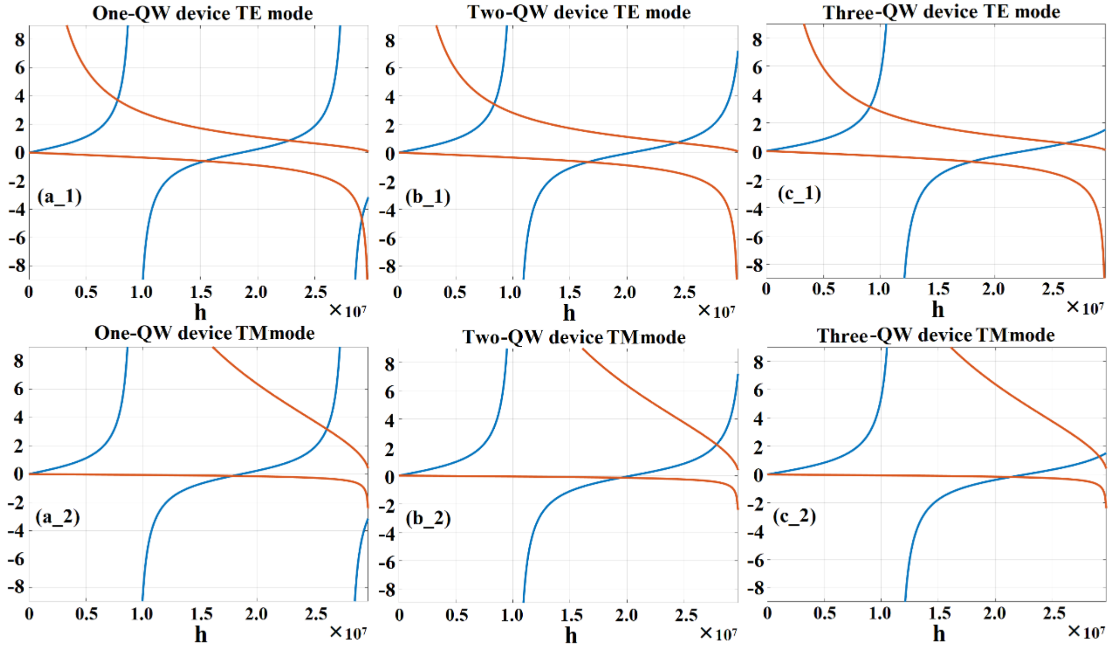

Figure 18. Waveguide mode. (a_1) and (a_2) are eigenvalue solution for one-QW device waveguide; (b_1) and (b_2) are eigenvalue solution for two-QW device waveguide; (c_1) and (c_2) are eigenvalue solution for three-QW device waveguide;

The number of mode supported by waveguides can be read directly from figure 18: waveguide for one-QW device supports 4 TE modes and 3 TM modes; waveguide for two/three-QW device supports 3 TE modes and 3 TM modes.

2.4.2. 3-D Model for Rib Waveguide Simulation

In order to learn the energy distribution in waveguide, 3D simulation on COMSOL simulation has been done. The model has been built is a GaN rib wrapped by air while the bottom satisfies scattering boundary condition to mimic the real condition on substrate. The height of the waveguide is 500nm.

Energy distribution at the exit end of waveguide is shown in figure 19. Therefore, the fin extended from the laser is a multimode waveguide, yet that is not what is supposed to see in parallel links: single mode transmission is more favorable for data communication. There are three methods to solve this problem: (i) The most direct way is to change the standing wave condition and choose a smaller q to shrink the cavity length. Correspondingly, the extended part will be smaller. (ii) Use longer wavelength: that means we need to shrink the band gap of quantum wells by increasing the Indium fraction, yet it can be difficult to achieve the high Indium fraction. (iii) We may only shrink the fin size of the extended part only, and in this way, the laser design is still valid, even though it brings about more complicated waveguide fabrication process.

The optimization of fin size will not be discussed further in this research, since the focus is on laser device. However, it will be a great progress in parallel links if decades nanometers waveguide can be applied to PIC industry.

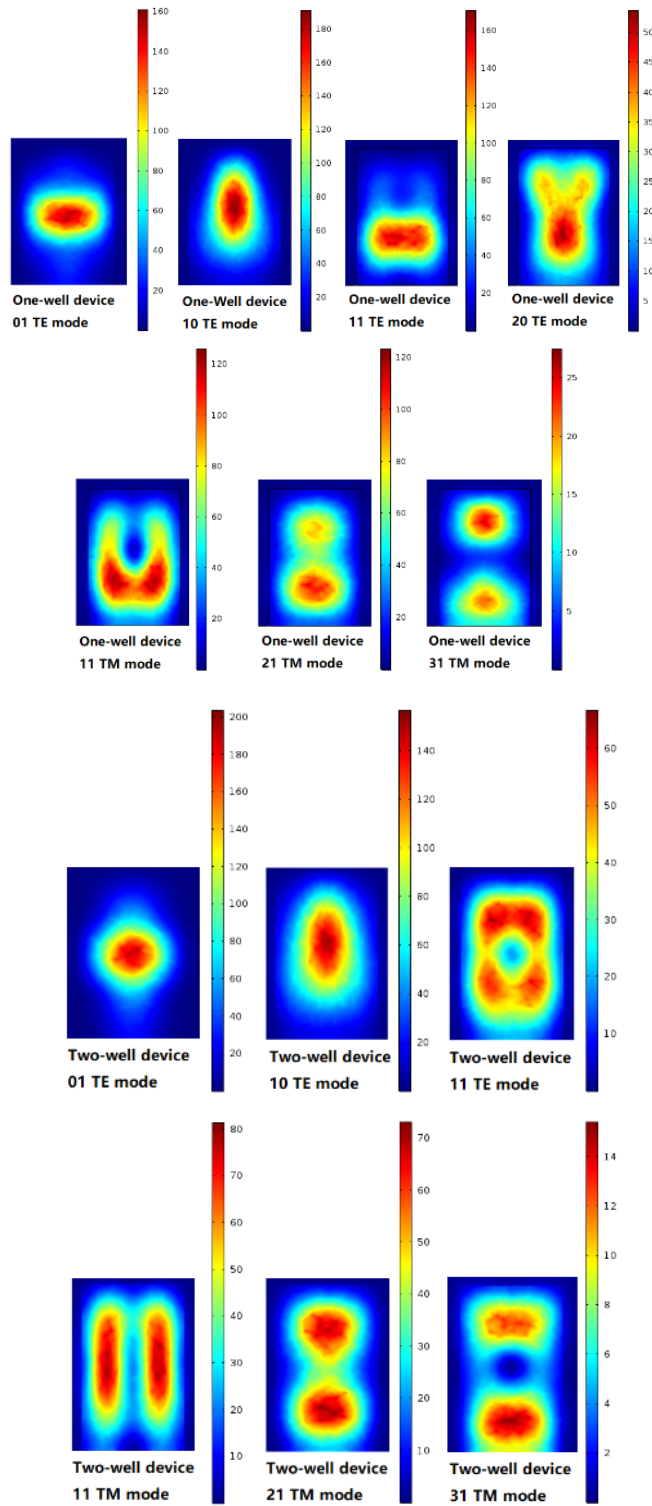

Figure 19. Energy distribution in waveguides

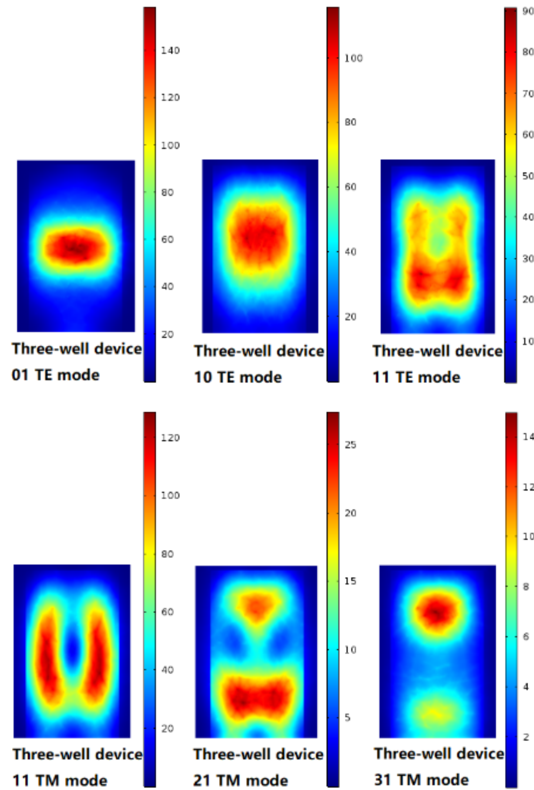

Figure 19. Continued

In summary, the design of one/two/three-QW device is finished, and the structure of the device has been quantized. Started from LED design, the internal quantum efficiency and the spectrum shows good performance; in DBR design, high-reflectance mirror has been made, and the upper boundary of reflectance is 99.97% if the absorption of internal p contact is taken into account; in cavity design, resonance can be observed, and the resonant frequencies match the peaks of LED spectrum, which is potential to achieve the optimal gain. So far, the device itself works well, however, this design is not perfect when considering the parallel link and PICs application, which prefers to single mode propagation. We provide three ways to enhance the quality of the fin. Nevertheless, the focus of this thesis

is the laser itself, and the optimal design and behavior in communication is another consideration, which will not be discussed further in this research. The priority first now is the performance of laser, which includes spectrum, threshold current, and gain.

References

[1] A. Zandi Goharrizi, Gh.Alahyarizadeh, Z.Hassan, H.AbuHassan, "Study on effect of quantum well number on performance characteristics of GaN-based vertical cavity surface emitting laser", Physica E 50 (2013) 61–66.

[2] Hongping Zhao, Guangyu Liu, Jing Zhang, et, al., "Approaches for high internal quantum efficiency green InGaN light-emitting diodes with large overlap quantum wells", Optics Express 4 July 2011, Vol. 19, No. S4, pp 991-1007.

[3] M. Molnár, D. Donoval, J. Kuzmík, et, al., "Simulation study of interface traps and bulk traps in n++GaN/InAlN/AlN/GaN high electron mobility transistors", Applied Surface Science 312 (2014), pp 157–161.

[4] H. Vilchis, V.D. Compeán-García, I.E. Orozco-Hinostroza, E. López-Luna, M.A. Vidal, A.G. Rodríguez, "Complex refractive index of $In_XGa_{1-X}N$ thin films grown on cubic (100) GaN/MgO", Thin Solid Films 626 (2017), pp 55–59.

[5] N. Antoine-Vincent, F. Natali, M. Mihailovic, et, al., "Determination of the refractive indices of AlN, GaN, and AlxGa1-xN grown on (111) Si substrates", Journal of Applied Physics, **93**(9), pp 5221-5226, 1 May 2003.

[6] Nurmikko, A., & Han, J. (2002). Blue and Near-Ultraviolet Vertical-Cavity Surface-Emitting Lasers. MRS Bulletin, **27**(7), 502-506. doi:10.1557/mrs2002.167.

[7] Maćkowiak, P., SarzaŁa, R., Wasiak, M. et al. "Cascade nitride VCSEL designs with tunnel junctions", Appl. Phys. A 78, 315–322 (2004).

3. FSML MODELLING AND DATA ANALYSIS

Even though the structures of FSMLs have been detailly described and well defined in chapter 2, the laser modelling is still a highly complex and challenging work: it is a multi-physics model which refers to electromagnetics and electrics, and the interaction of light and electric behavior can be difficult to make sense. In this chapter, we start from multi-physics simulation which includes optics and semiconductor module to get modal gain and reduce the complex multi-physics problem to be a pure optical problem to get the laser performances and data analysis.

3.1. Optical Gain

3.1.1. Gain and Absorption in Laser Media

Three types of transition occur in the active region when a VCSEL works: spontaneous emission, stimulated emission and absorption. Spontaneous emission is the dominate process in LEDs. When current injected across a forward-biased junction, recombination occurs; and if the material is direct semiconductor, the energy released in recombination is going to be in the form of electromagnetic waves, and this process is spontaneous emission. Figure 20 is spontaneous emission process in band structure. As it is shown, since electrons in many different energy levels take part in this process, the wavelength of generated light ranges from low to high, therefore, the spectrum of spontaneous emission is relatively wide. In FSMLs, this process provides a “light pump” for stimulated emission.

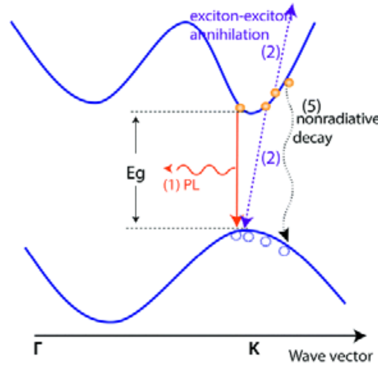

Figure 20. Spontaneous emission in direct semiconductor [1]

When light goes across the forward-biased junction, stimulated emission and absorption occurs simultaneously: light can induce the electrons in conduction band downward and recombined with holes in valence band, and it can also break some of the hole-electron pairs and excites electrons upward to conduction band. The former process is stimulated emission, which amplify the light at certain wavelength. Figure 21 presents the principles of semiconductor laser.

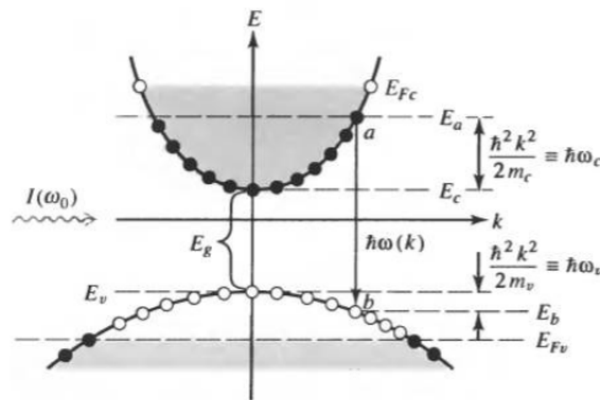

Figure 21. Principles of semiconductor laser [2]

Transition energy (for both absorption and stimulated emission), according to figure 21, can be expressed as:

$$\hbar\omega_0 = E_g + \frac{\hbar^2 k_0^2}{2m_c} + \frac{\hbar^2 k_0^2}{2m_v}$$

and the optical gain in this interaction is:

$$\gamma(\omega_0) = \frac{\lambda_0^2}{8\pi^2 n^2 \tau}\left(\frac{2m_c m_v}{\hbar(m_c + m_v)}\right)^{3/2}\left(\omega_0 - \frac{E_g}{\hbar}\right)^{1/2}[f_c(\omega_0) - f_v(\omega_0)]$$

where ω_0 is the photon energy of input light; n is refractive index of emission material; τ is the lifetime of electrons in conduction band; $\hbar$ is planck's constant; m_c and m_v are effective mass in conduction band and valence band; $f_c(\omega_0)$ and $f_v(\omega_0)$ are Fermi-Dirac functions.

3.1.2. Gain in QW Lasers

Different from the conventional bulk material laser, material gain of QW laser is quantized, and it should be described by:

$$\gamma(\omega_0) = \frac{m_r \lambda_0^2}{4\pi\hbar L_z n^2 \tau}[f_c(\hbar\omega_0) - f_v(\hbar\omega_0)]\sum_{l=1}^{\infty} H(\hbar\omega_0 - \hbar\omega_l)$$

where $\mathrm{H}(x)$ is the Heaviside function, and if x>0, $\mathrm{H}(x) = 1$; if x<0, $\mathrm{H}(x) = 0$. L_z is the width of quantum well; m_r is described as $\frac{m_c m_v}{(m_c + m_v)}$; and l represent the subband of emission quantum well.

With the knowledge of the gain and absorption, let's turn to the case of our device. Gain calculation in COMSOL software is a multi-physics problem which includes electromagnetic wave module and semiconductor module. The gain function provided by COMSOL is conventional material gain, which is not a precise description of for this research. This problem can be solved by more advanced and professional tools such as

Crosslight. Yet here we only do the rough estimation and try to make sense when the gain is able to overcome the attenuation due to the optical loss.

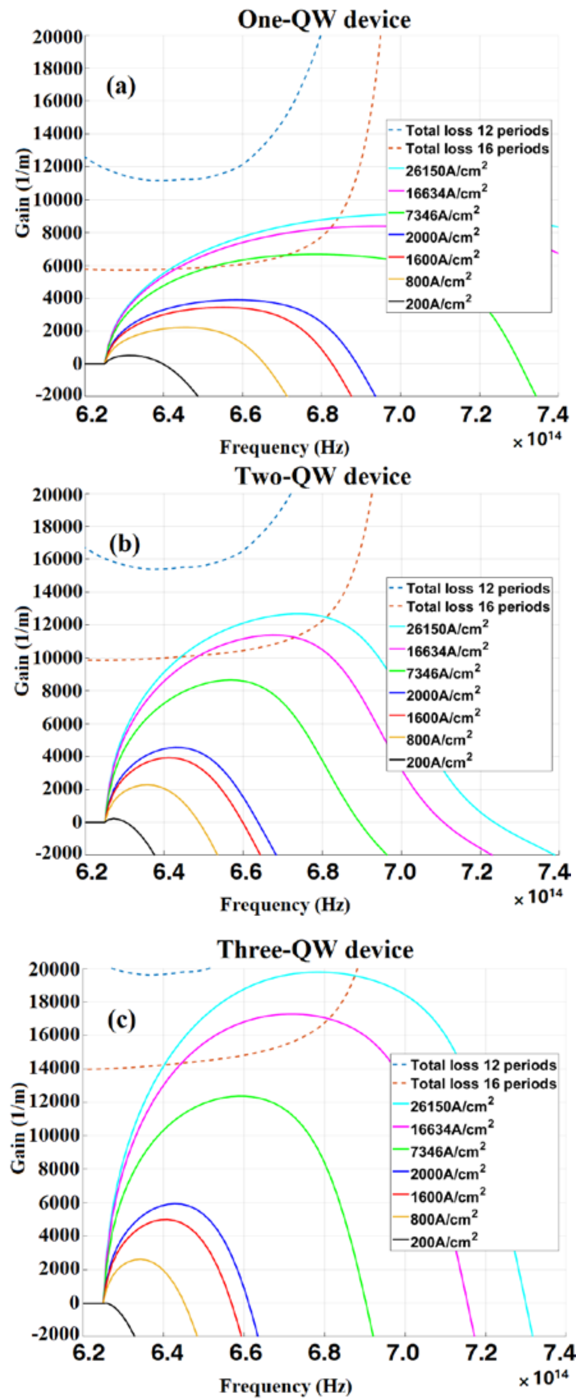

Figure 22. Modal gain (1/m) of QWs in currents. (a) one-QW device; (b) two-QW device; (c) three-QW device

Figure 22 presents the modal gain of QWs (solid lines) and the total loss in the cavity (dash lines). The total loss includes the loss on DBRs and material absorption. As observed, material gain in one-QW device (a) is larger than others at the same current bias, and that is because the carrier density in that QW is larger than the other two. If the number of DBR periods is small (<16), the modal gain can hardly compensate the power loss so that threshold gain is going to be larger. All gain curves are started from zero in low frequency, and that is because when $\hbar\omega_0$ is smaller than E_g, there is no electric transition at these energies. As the frequency goes larger, gain turns to be positive, and that means the amplification of light. However, when the frequency goes even larger, gain curves goes down, and theoretically at the point of $h\nu = E_{Fc} - E_{Fv}$, where ν is frequency, gain drops to zero, and if continually increase the frequency, the light power will be absorbed.

Some literatures compare the modal gain of bulk material laser and quantum well laser and present the profiles of both cases. A direct observation is that based on the same materials, the maximum of quantum well laser gain shows up earlier than that of bulk material gain, shown in figure 23 [4]. That indicates that if more precise model is applied in our device, the leasing condition should be easier to satisfy because the modal gain curve will get intersected with loss curve before the frequency of 6.4e14Hz in figure 22 (a) (b) (c).

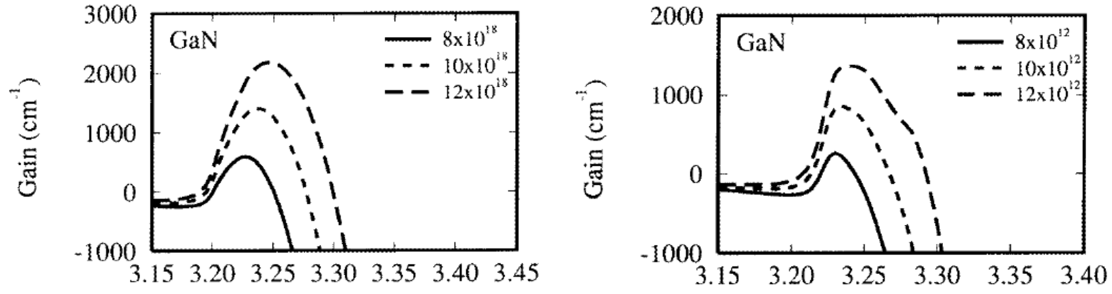

Figure 23. Modal gain of bulk GaN laser (left) and QW GaN laser(right), reprinted from [4]

In terms of power loss, it increases as the active region gets larger, and this increase the difficulties for lasers to reach their threshold gain. As observation, the one-QW laser reaches its threshold with the bias of 7346 A/cm^2; while the bias required by other two lasers are much larger (above 10000A/cm^2).

3.2. A General Method for Semiconductor Laser Modelling

The purpose of this section is to do the laser simulation. With the knowledge of the previous section, we know that the behaviors of electrons and photons in QWs include spontaneous emission, stimulated emission, and semiconductor absorption. However, we are still curious about how these behaviors work together to get the laser spectrum. So far, there are three factors that determines the selective amplification of wavelength: DBR, which confines certain range of wavelength; cavity length, which is able to select the resonant frequency to amplify; gain-absorption curves, which amplify some light while absorb others. What is also necessary to pay attention to is that the total absorption in device is not just caused by the semiconductor, but extinction coefficient in complex refractive index as well, so it also contribute to the selective absorption. In this section, we can learn

how to use these four factors and COMSOL software to determine laser spectrum.

3.2.1. Effective Extinction Coefficient

The most direct way to do laser simulation is to follow the physical steps. When current injects into the device, the first photon generated by the laser must be a spontaneous-emission photon because there is no light-stimulation for stimulated emission so far. The first photon, with its "brothers" generated simultaneously, has several ways to go: it can be absorbed because of extinction coefficient and QW; or it can struggle through DBRs and escape; and another way is that it will be confined in the cavity and take part in stimulated emission. These pioneer-photons spend some time (although extremely fast for human beings) to disturb the "unstable" electrons hanging in the conduction band and induce them downwards to react with the holes waiting "below" to generate stimulated photons. Considering the current are injecting constantly, at this moment, the light remained in the cavity are consisted of spontaneous-emission photons and the first generation of stimulated-emission photons. Since then, stimulated emission and spontaneous emission keep going without any interruption, and light power in the cavity goes larger and larger until converged. This process can be described with the flow chart in figure 24:

However, if we focus on the motion of photons, a challenge we have to encounter is that process ① is an almost endless loop before the power is converged. Therefore, this flow chart cannot be translated to be an efficient computer program.

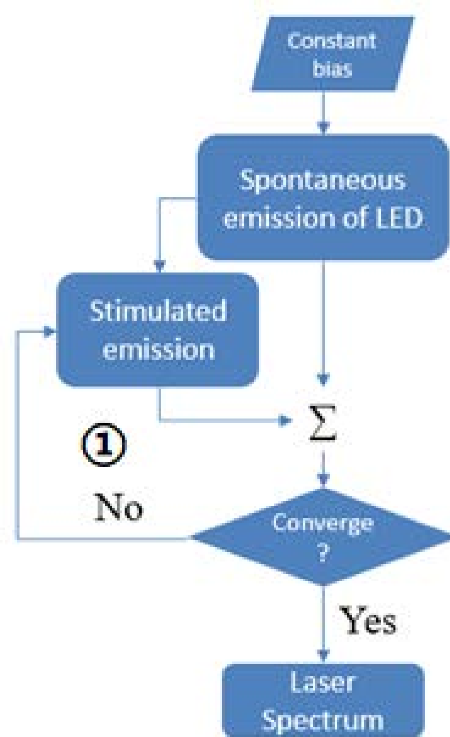

Figure 24. Flow chart physical description of laser model

Physically speaking, process ① is complex, but it can be very simple mathematically, and the mathematical expression of it has been formulated and visualized already: gain-absorption curves. Naturally, considering the unit of gain and semiconductor absorption, these two factors can be combined with extinction coefficient, and the process is shown below:

Assume a light beam with the power of P_0 is propagating in the cavity without hitting on DBRs; when it goes through certain distance L, the power remained should obey beer's law:

$$P_1 = P_0 e^{gL} e^{-\beta L}$$

where g is gain when it is positive, and semiconductor absorption when it is negative, and

β is absorption caused by extinction coefficient:

$$\beta = \frac{4\pi\kappa}{\lambda_0}$$

therefore:

$$P_1 = P_0 e^{\frac{-4\pi L}{\lambda_0}(\kappa - \frac{\lambda_0 g}{4\pi})}$$

We name $\kappa - \frac{\lambda_0 g}{4\pi}$ as effective extinction coefficient, k_{eff}, and this variable can fully present the power change of the light beam in cavity. Figure 27 shows that how k_{eff} changes with current.

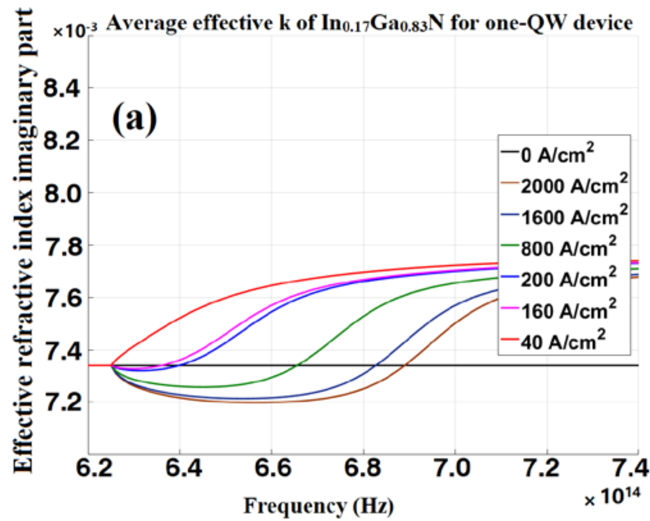

Figure 25. Average effective extinction coefficient of QWs. (a) one-QW device; (b) two-QW device; (c) three-QW device

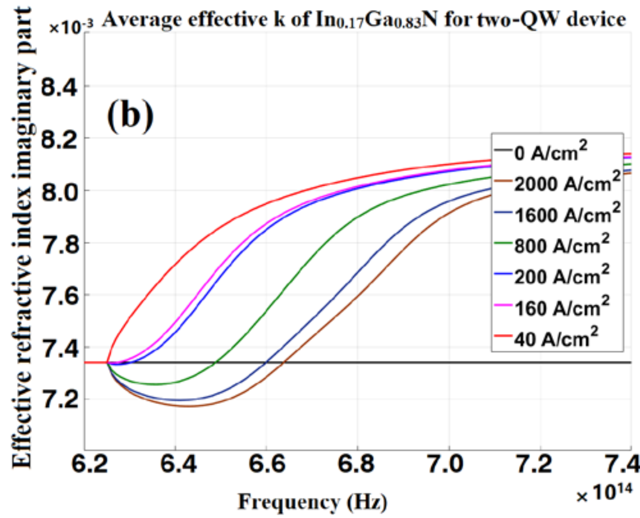

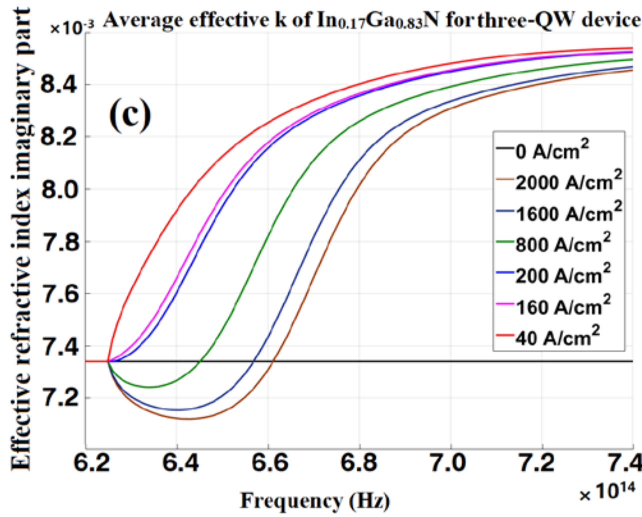

Figure 25. Continued

According to figure 25, when injection current is very small, the effective extinction coefficient is larger than extinction coefficient, yet as the current goes larger, a certain range of effective extinction coefficient curve is pulled down, and when the current is sufficiently large, effective extinction coefficient can be smaller than extinction coefficient at certain range, and that means the optical gain compensates some of the absorption. If the gain is larger than all the power loss in cavity, light output will be amplified.

3.2.2. "Pure Optical" Model

Effective extinction coefficient is a very important concept in this simulation study; it contains the information of optical amplification and absorption while successfully avoid the complex physical process of stimulated emission and spontaneous emission. Therefore, we can reduce the complex multi-physics problem to be a pure optical problem, and the only change is the imaginary part of refractive index, which is replaced by effective extinction coefficient.

3.3. Performance of One/Two/Three-MQW FSML

Since we know the spectrum of LED and amplification and absorption and transmission/reflection that light can experience, we are close to the final results. LED spectrum is used as the pumping source of the laser, and effective extinction coefficient replace extinction coefficient, and the structures are in table 4. In order to reduce the power loss in device, I adopt 16-period DBRs so that the modal gain can compensate the power loss for each round.

3.3.1. Quality Factor of FSMLs Spectrum

The spectrum of laser, based on "pure optical model", is presented in figure 26.

In figure 26, the peaks of these devices show up at different positions, which means the resonant frequency (f_{re}) are different: for one-QW device, f_{re} is 461.22nm; for two-QW device, it is 459.1nm; and for three-QW device, it is 457.7nm. This shift is caused by the linearly variation of refractive index distribution in cavity.

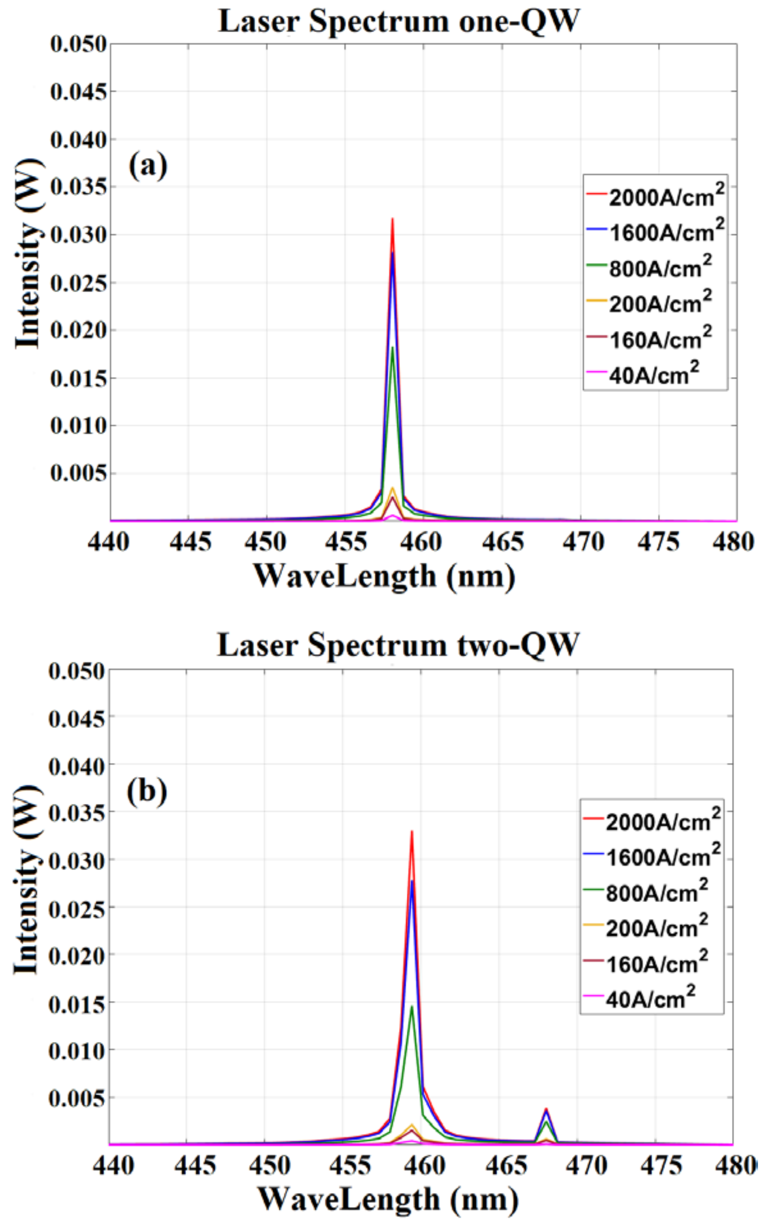

Figure 26. Spectrum output of laser. (a) one-QW device; (b) two- QW device; (c) three- QW device

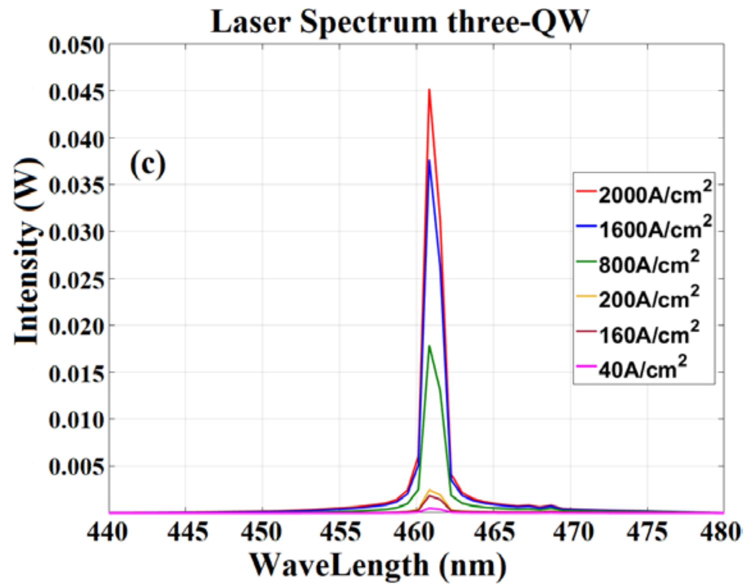

Figure 26. Continued

FWHM (full width at half maxima) and quality factor (Q) are very important parameters to evaluate the quality of the laser, which can be read from figure 26. FWHM and quality factor are shown in figure 27 and figure 28 respectively.

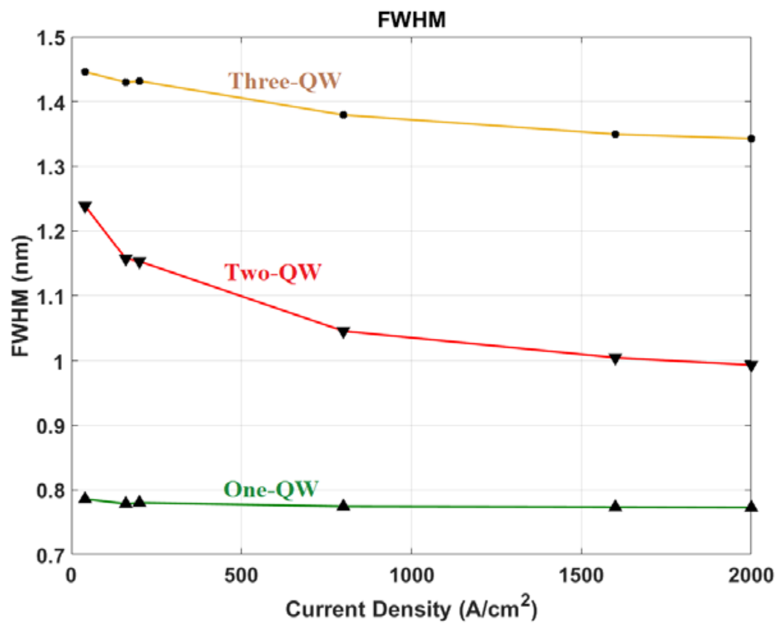

Figure 27. FWHM vs. Current Density

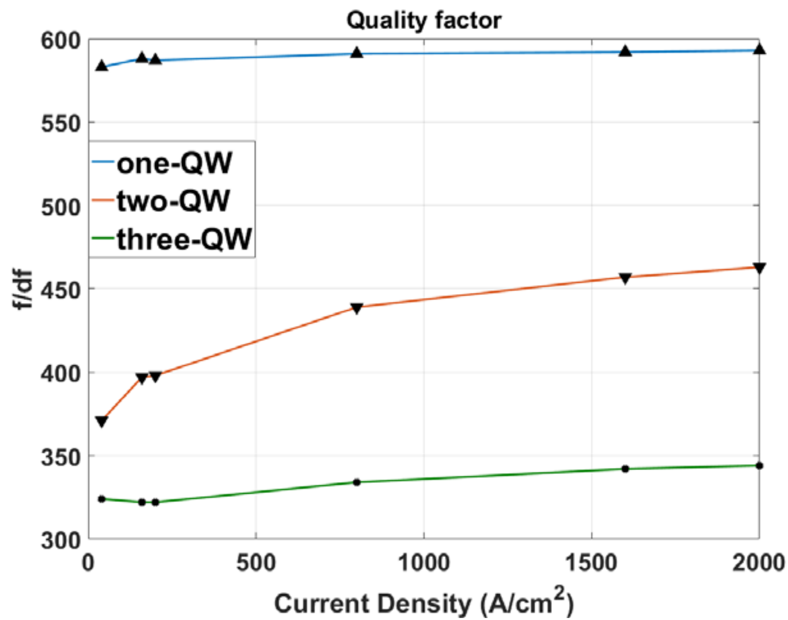

Figure 28. Quality factor vs. Current Density

A direct observation of the performances of these devices is that the one-QW device has the largest quality factor even though the power remained in cavity is relatively weak. The large spontaneous emission rate leads to the large power output of three-QW laser, yet since the quality factor of this cavity is less than that of one-QW device, its FWHM is wider.

3.3.2. Threshold Current of FSMLs

One of the advantages of FSML is its very low threshold current. Active region of conventional VCSELs are sandwiched by semiconductor DBRs, and the injecting current unavoidably, has to go through DBRs. In this way, the threshold current of VCSELs has to be very large. However, in our design, we can take advantage of internal electrode so that current can be injected into active regions directly. Plus, we can also reduce the threshold current by reduce the threshold gain, which is determined by power loss in laser, the

relationship between threshold gain and current are presented as:

$$I_{th} \propto e^{g_{th}}[3]$$

Figure 29 shows the power output as a function of current density. The data can be read directly from figure 26, and threshold current density for the three devices are all smaller than 200A/cm^2, which is 1mA in current.

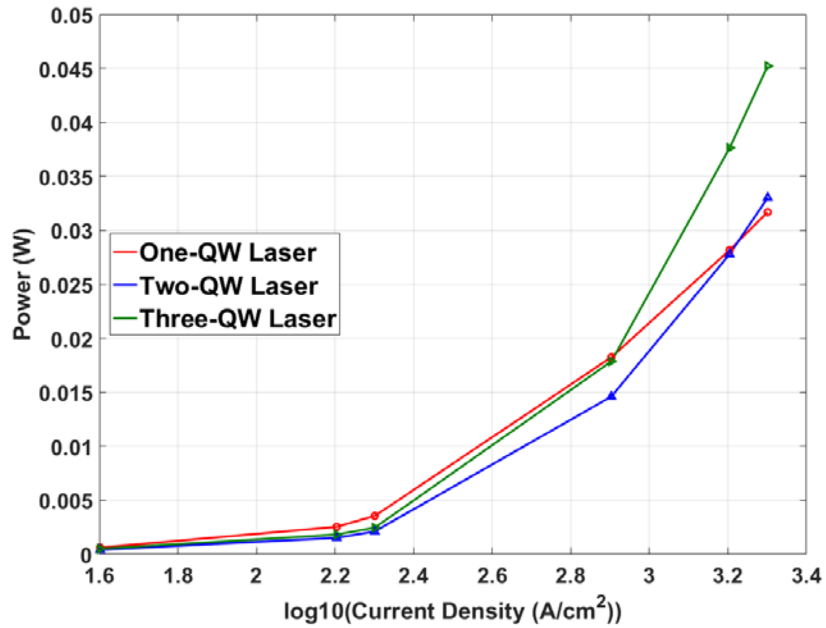

Figure 29. Laser power output as a function of current density

References

[1] L. Yuan and L. Huang, "Exciton dynamics and annihilation in WS 2 2D semiconductors," Nanoscale 7, 7402–7408 (2015).

[2] Amnon Yariv, Pochi Yeh, Photonics: Optical Electronics in Modern Communications (The Oxford Series in Electrical and Computer Engineering), Oxford University Press, Inc., New York, NY, 2006.

[3] R. Michalzik Ed., VCSELs—Fundamentals, Technology and Applications of Vertical-Cavity Surface-Emitting Lasers. Springer Optical Sciences Series, vol. 166. Berlin, Germany: Springer-Verlag, 2013.

[4] A T Meney, E P O'Reilly and A R Adams, Optical gain in wide bandgap GaN quantum well lasers, Semicond. Sci. Technol. 11 (1996) 897–903.

4. CONCLUSION AND FUTURE DIRECTION

In this research, we figured out an instructive method to design a FSML with the consideration of DBRs, cavity, LED, and fin. In order to see the laser performance, we put forwards the concept of effective extinction coefficient to reduce the complex multi-physics problem to be a pure optical simulation, which dramatically shorten the simulation time and lower the computer memory requirement. Depended on the 2D simulation, we basically learned the laser performance, which shows small threshold current and large power in the fin.

4.1. Limitations of Simulation Work and Outlook

There are several technical details in our simulation work that can cause inaccuracy in simulation results: (I) gain curve of COMSOL is depended on bulk material, which is instructive on the design, but not precise for performance. In order to fully understand the performance of device and the quantum well active regions, we need more advanced software such as Crosslight and Synopsys; (II) coefficients applied in this research are all provided by reference; however, since the materials grown in our lab may have different quality with theirs, the coefficients need to be revised based on experiments; (III) sweeping frequency in our simulation are periodical discrete impulse instead of continuous spectrum, thus the laser spectrum can be not accurate: maxima cannot be observed if it is located between two consecutive frequencies, and in this way, the maxima we measured can be

lower than the real one; (IV) 2D simulation is not able to fully reflect the performance of FSML. Figure 24 describes the path that light can escape from the cavity. In 2D simulation, we don't need to consider the propagation in waveguide direction, therefore, light source in laser can be confined between two DBRs and gets fully "reshaped" as process ① in figure 24, and we assumed the power output in the 2D model is the spectrum we want to get. However, in real device, photons are free in the direction of waveguide, so that some of the photons can go into the waveguide without being fully "reshaped", therefore, the signal in waveguide is not only the laser spectrum, it also includes the incompletely developed LED light, which can lower the quality factor of laser signal, and this path is ③ in figure 30.

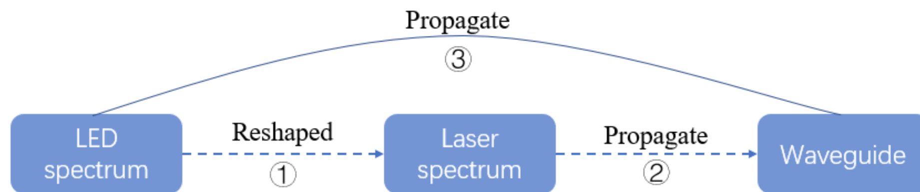

Figure 30. Light propagating in device

With the knowledge of that, we can predict that the FSML we designed can be a compromising between a VCSEL and a EELD, hopefully, we can go forward in 3D simulation, or confirm the assumption by fabrication.

4.2. Further Plan: Research Focus in PhD Period

In my academic plan, I want to pursue a PhD degree after graduation. It will be great if I can continue this research in my advisor, Dr. Harris' group. When I pursue my master degree, I have acquired fundamental knowledge background including electromagnetic theory, semiconductors, quantum mechanics, optics and optoelectronic theory, and basic

fabrication skills including sputtering, CVD, lithography, thermal diffusing and etching, and basic computer software skills such as COMSOL multi-physics, MATLAB, Autodesk Inventor, and Microsoft Office software. Although these skills are far less sufficient to support my goal, they are helpful for me to start my academic career. I want to achieve the device I designed, and if my efforts can provide any ideas for photonic integrated circuit designers or make any contribution in this industry, I will feel a sense of achievement.